

University of Szeged

Faculty of Pharmacy

Institute of Pharmaceutical Technology and Regulatory Affairs

Head: Prof. Dr. Ildikó Csóka Ph.D.

Ph.D. Thesis

**DEVELOPMENT OF ISONIAZID LOADED NANOTECHNOLOGY-
BASED DRY POWDER PULMONARY FORMULATIONS FOR
TREATMENT OF TUBERCULOSIS**

Mahwash Mukhtar

Pharm. D., M.Phil.

Supervisor:

Dr. Habil. Rita Ambrus Ph.D.

SZEGED

2022

PUBLICATIONS RELATED TO THE SUBJECT OF THE THESIS

1. **Mukhtar Mahwash**, Hussain Ali, Naveed Ahmed, Rashid Munir, Sumbal Talib, Anam S. Khan, and Rita Ambrus. "Drug delivery to macrophages: A review of nano-therapeutics targeted approach for inflammatory disorders and cancer." *Expert Opinion on Drug Delivery* 17(9) (2020): 1239-1257. (Q1)
2. **Mukhtar Mahwash**, Edina Pallagi, Ildikó Csóka, Edit Benke, Árpád Farkas, Mahira Zeeshan, Katalin Burián, Dávid Kókai, and Rita Ambrus. "Aerodynamic properties and in silico deposition of isoniazid loaded chitosan/thiolated chitosan and hyaluronic acid hybrid nanoplex DPIs as a potential TB treatment." *International Journal of Biological Macromolecules* 165 (2020): 3007-3019. (Q1)
3. **Mukhtar Mahwash**, Eszter Fényes, Csilla Bartos, Mahira Zeeshan, and Rita Ambrus. "Chitosan biopolymer, its derivatives and potential applications in nano-therapeutics: A comprehensive review." *European Polymer Journal* 160 (2021): 110767. (Q1)
4. **Mukhtar Mahwash**, Zsolt Szakonyi, Árpád Farkas, Katalin Burian, Dávid Kókai, and Rita Ambrus. "Freeze-dried vs spray-dried nanoplex DPIs based on chitosan and its derivatives conjugated with hyaluronic acid for tuberculosis: *In vitro* aerodynamic and *in silico* deposition profiles." *European Polymer Journal* 160 (2021): 110775. (Q1)
5. **Mahwash Mukhtar**, Noemi Csaba, Sandra Robla, Rubén Varela-Calviño, Attila Nagy, Katalin Burian, Dávid Kókai and Rita Ambrus. "Dry powder comprised of isoniazid loaded nanoparticles of hyaluronic acid in conjugation with mannose anchored chitosan for macrophage targeted pulmonary administration in Tuberculosis." *Pharmaceutics* (under review) (Q1)
6. Ildikó Csóka, Keyhaneh Karimi, **Mahwash Mukhtar**, and Rita Ambrus. "Pulmonary drug delivery: Role of antibiotic formulations for treatment of respiratory tract infections". *Acta Pharmaceutica Hungarica* 89(2) (2019): 43-62. (Q4)

PRESENTATIONS RELATED TO THE SUBJECT OF THE THESIS

1. **Mahwash Mukhtar** and Rita Ambrus. “Fabrication of pulmonary formulations containing hyaluronic acid and chitosan-based nanoparticles for drug delivery in tuberculosis”. I-Symposium of Young Researchers on Pharmaceutical Technology, Biotechnology and Regulatory Science. p. 5. (2019)
2. **Mahwash Mukhtar** and Rita Ambrus. “Development of Inhalable Chitosan nano system conjugated with Hyaluronic acid for treatment of Tuberculosis”. II-Symposium of Young Researchers on Pharmaceutical Technology, Biotechnology and Regulatory Science. p. 38. (2020)
3. **Mahwash Mukhtar** and Rita Ambrus. “Fabrication of isoniazid loaded chitosan/thiolated chitosan and hyaluronic acid hybrid nanoplex DPIs as a potential TB treatment: Aerodynamic properties and *in silico* deposition in lungs”. EUGLOH Annual Student Research Conference (2020)
4. **Mahwash Mukhtar** and Rita Ambrus. “A Design of Experiment (DoE) approach for the chitosan/thiolated chitosan and hyaluronic nanoplexes for the pulmonary drug delivery in tuberculosis”. Medical Conference for PhD Students and Experts of Clinical Sciences. p. 38. (2020)
5. **Mahwash Mukhtar** and Rita Ambrus. “Spray dried hyaluronic acid nanoplexes conjugated with chitosan and its derivatives for the pulmonary administration as dry powder inhalers for tuberculosis”. III-Symposium of Young Researchers on Pharmaceutical Technology, Biotechnology and Regulatory Science. p. 16. (2021)
6. **Mahwash Mukhtar** and Rita Ambrus. “*In silico* and *in vitro* aerodynamic profile of chitosan/thiolated chitosan and hyaluronic acid hybrid nanoplex based DPIs for tuberculosis”. Journal of aerosol medicine and pulmonary drug delivery 34(3) pp. A11-A12. DOI: 10.1089/jamp.2021.ab01.abstracts (2021).
7. **Mahwash Mukhtar**, Noemi Csaba, Sandra Robla and Rita Ambrus. “Mannosylated chitosan-based pulmonary drug delivery system for targeting macrophages”. IV-Symposium of Young Researchers on Pharmaceutical Technology, Biotechnology and Regulatory Science. p. 28. (2022)

ABBREVIATIONS

ACI	Andersen Cascade Impactor
AM	Alveolar macrophages
BB	Box-Behnken
BH	Breath-hold
CD80-PE	Phycoerythrin-conjugated anti-human CD80
CD83-APC	Allophycocyanin-conjugated anti-human CD83
CLSM	Confocal laser scanning microscope
CMA _s	Critical material attributes
COPD	Chronic obstructive pulmonary disease
CPP _s	Critical Process Parameters
CQA _s	Critical Quality Attributes
CS	Chitosan
CSM	Chitosan/hyaluronic acid nanopowder with mannitol
CSI400	Chitosan/hyaluronic acid nanopowder with InhaLac [®] 400
DAPI	4',6-diamidino-2-phenylindole
DMEM	Dulbecco's Modified Eagle Medium
DoE	Design of Experiment
DPI _s	Dry powder inhalers
DSC	Differential Scanning Calorimetry
EDAC	(1-ethyl-3-(3-dimethylamino propyl) carbodiimide hydrochloride)
EE	Encapsulation efficiency
EMA	European Medicines Agency
ET	Fraction in the extra-thoracic airways
EXH	Exhaled fraction
FBS	Fetal bovine serum
FDA	U.S. Food and Drug Administration
FPF	Fine particle fraction
FTIR	Fourier Transform Infrared Spectroscopy
GM-CSF	Granulocyte-Macrophage Colony-Stimulating Factor
HA	Hyaluronic acid

HPMC	Hydroxy propyl methylcellulose
ICH	International Council for Harmonization
IDO	2,3-Indoleamine dioxygenase
INH	Isoniazid
INH-CS/HA NPs	Isoniazid loaded chitosan and hyaluronic acid hybrid nanoparticles
INH-MC/HA NPs	Isoniazid loaded mannosylated chitosan and hyaluronic acid hybrid nanoparticles
I400	InhaLac [®] 400
LUNG	Cumulative fraction deposited in the bronchial and acinar region
MC	Mannosylated chitosan
MCM	Mannosylated chitosan/hyaluronic acid nanopowder with mannitol
MCI400	Mannosylated chitosan/hyaluronic acid nanopowder with InhaLac [®] 400
MFI	Mean fluorescence intensity
min	Minute
MMAD	Mass median aerodynamic diameter
M.Tb	Mycobacterium tuberculosis
MTT	3-(4,5-dimethylthiazol-2-yl)-2,5 diphenyltetrazolium bromide
MTS	3-(4,5-dimethylthiazol-2-yl)-5-(3-carboxymethoxyphenyl)-2-(4-sulfophenyl)-2H-tetrazolium
NGI	Next generation impactor
NPs	Nanoparticles
OD	Optical density
PBMC	Peripheral Blood Mononuclear Cells
PBS	Phosphate buffer saline
PDI	Polydispersity index
PLC	Programmable logic controller
pMDIs	Pressurized meter dose inhalers
PSG	Penicillin-Streptomycin-Glutamine
QbD	Quality by Design
QTPP	Quality Target Product Profile
RBCs	Red blood cells
Rh-B	Rhodamine-B

Rh-B CS/HA NPs	Rhodamine-B loaded chitosan and hyaluronic acid hybrid nanoparticles
Rh-B MC/HA NPs	Rhodamine-B loaded mannosylated chitosan and hyaluronic acid hybrid nanoparticles
RPMI-1640	Roswell Park Memorial Institute medium-1640
SDS	Sodium dodecyl sulfate
SEM	Scanning Electron Microscope
SLF	Simulated lung fluid
TB	Tuberculosis
TC	Thiolated chitosan
TGA	Thioglycolic acid
Th1	Helper T cell 1
TPP	Sodium tri-polyphosphate
UN	United Nations
WHO	World Health Organization
XRPD	X-ray Powder Diffraction

TABLE OF CONTENTS

1. INTRODUCTION	1
2. AIMS.....	2
3. LITERATURE BACKGROUND.....	3
3.1 Pharmaceutical and immunological aspects	3
3.1.1 Pathogenesis of Tuberculosis.....	3
3.1.2 Limitations to the treatment of Tuberculosis	3
3.1.3 Various pulmonary drug delivery mechanisms using different devices.....	5
3.1.4 Nanotechnology as a new paradigm in pulmonary drug delivery	7
3.1.5 Polymeric nanoparticles for the delivery of anti-tubercular drugs	9
3.1.5.1 Chitosan and its derivatives	10
3.1.5.2 Hyaluronic acid	10
3.1.6 Drying methods to obtain DPIs.....	11
3.1.6.1 Methods for developing DPIs by freeze-drying	11
3.1.6.2 Methods for developing DPIs by spray-drying.....	12
3.2 Regulatory aspects	12
3.2.1 Quality by Design approach.....	12
3.2.2 Design of Experiment (DoE)	14
4. MATERIALS AND METHODS	14
4.1 Materials	14
4.2 Method.....	17
4.2.1 Synthesis of polymer.....	17
4.2.2 Quantification of polymer	17
4.2.3 Characterization of polymer	18
4.2.4 Application of QbD.....	18
4.2.4.1 Knowledge space development and defining quality target product profile (QTPP).....	18
4.2.4.2 Determining CQAs, CPPs, and CMAs.....	18
4.2.4.3 Initial risk assessment	19
4.2.5 Design of Experiment	19
4.2.6 Preparation of nanosuspensions	19
4.2.7 Preparation of dry powders	20

4.2.7.1 Freeze-drying to obtain nanopowders	20
4.2.7.2 Spray-drying to obtain nanopowders.....	21
4.2.8 Drug loading (Percentage encapsulation efficiency)	21
4.2.9 Morphological, micrometric investigation and characteristics of powder.....	21
4.2.10 Physico-chemical investigations	22
4.2.10.1 Fourier transform infrared spectroscopy	22
4.2.10.2 X-ray powder diffractometry.....	22
4.2.10.3 Differential Scanning Calorimetry	22
4.2.11 <i>In vitro</i> studies.....	23
4.2.11.1 Drug release study	23
4.2.11.2 Permeation study	23
4.2.11.3 Aerodynamic profile.....	23
4.2.12 <i>In silico</i> studies	24
4.2.13 Colloidal stability in culture media.....	25
4.2.14 Cell cultures	25
4.2.15 Macrophage isolation from human blood	25
4.2.16 <i>Ex vivo</i> studies.....	26
4.2.16.1 Cytotoxicity studies	26
4.2.16.2 Blood compatibility study	27
4.2.16.3 Cellular uptake of nanopowders (<i>Qualitative and quantitative</i>)	27
4.2.16.4 Macrophage phenotype analysis.....	28
4.2.16.5 Tolerogenic activity of NPs.....	28
5. RESULTS AND DISCUSSION	29
5.1 Synthesis, quantification, and characterization of polymer.....	29
5.2 QbD and knowledge space of nanosuspensions	29
5.3 DoE for optimization of nanosuspensions.....	30
5.4 Drug loading (Percentage encapsulation efficiency).....	33
5.5 Morphological investigation and characteristics of powder.....	34
5.6 Outcomes of physicochemical investigation	35
5.6.1 Fourier transform infrared spectroscopy.....	35
5.6.2 X-ray powder diffractometry	36
5.6.3 Differential Scanning Calorimetry.....	37
5.7 Results of <i>In vitro</i> studies	38

5.7.1 Drug release study.....	38
5.7.2 Permeation study.....	38
5.7.3 Aerodynamic profile	39
5.8 Discussion of <i>in silico</i> studies	41
5.9 Results of colloidal stability in culture media	41
5.10 Evaluation of <i>ex vivo</i> studies	42
5.10.1 Cytotoxicity studies	42
5.10.2 Blood compatibility study.....	44
5.10.3 Uptake of nanopowders by macrophages (Qualitative and quantitative)	44
5.10.4 Macrophage phenotype analysis	45
5.10.5 Tolerogenic activity of NPs	46
6. CONCLUSION	48
7. NOVELTY AND PRACTICAL ASPECTS	50
8. REFERENCES.....	51
9. ACKNOWLEDGMENTS.....	59

1. INTRODUCTION

Tuberculosis (TB) is the leading cause of death of over 1.5 million people annually across the globe and the second leading infectious disease after COVID-19 pandemic, according to the statistics by the world health organization (WHO). At present, multidrug-resistant TB remains a public health crisis in undeveloped countries due to compromised socio-economic conditions (WHO, 2021). Lungs are the primary site for *Mycobacterium tuberculosis* (M.Tb) infection which is a facultative intracellular bacterium. M.Tb gains access to the lungs by inhalation of infected air droplets from the cough of an infected person. Following inhalation, M.Tb interacts with the mucous secreting goblet cells and some of the infected particles bypass the mucociliary system and, ultimately enter into the alveoli. During this pathogenesis, M.Tb is taken up by the alveolar macrophages (AM) using the ligand lipoarabinomannan. This ligand of the bacterium interacts with the mannose surface receptors of the AM to gain access to the macrophages where it resides and multiplies in the phagocytes [1]. M.Tb interacts with the T-lymphocytes to differentiate macrophages into granulomas characterized by the infiltration of inflammatory mononuclear cells. Later, the T-lymphocytes (effector cells) produce cytokines to facilitate the activation of previously infected macrophages to kill the M.Tb residing inside. Hence, T-cell response and activation are essential to the immune regulation in TB [2].

TB is curable but the ineffective management, high costs of therapy, and patient incomppliance contribute to the alarming rise in cases in this modern era. Hence, a cost-effective and patient-friendly drug delivery approach is essential to the treatment of TB. Development of the rational patient-friendly pharmaceutical dosage form is the time consuming and extensive work. However, the use of robust regulatory guidelines can minimize the development time of the dosage form without compromising quality by following the European Medicines Agency (EMA) and U.S. Food and Drug Administration (FDA) protocols at various steps. The quality by design (QbD) method is one such systematic approach and effective application that takes into consideration every aspect of product quality attributes during the early stage of dosage development whereas the design of experiment (DoE) facilitates the optimization of a pharmaceutical formulation [3].

2. AIMS

As the traditional therapy for TB fails to deliver the drug effectively to the target site and therefore suffers limitations in terms of bacterial resistance and patient non-compliance. Thus, the primary aim of this Ph.D. work was to fabricate and investigate the anti-tubercular isoniazid (INH) loaded nanotechnology-based dry powders for inhalation (DPIs) for targeted drug delivery. Polymers were chosen after a thorough review to successfully achieve the targeted delivery to the macrophages. The experimentally influential variables were also studied to demonstrate their effect on the final product, i.e., DPIs. Altogether, the study was aimed to not interfere with the natural immune response of the body and therefore cell culture-based studies were conducted to serve the purpose.

This Ph.D. work was designed and studied in the following parts, following the step-by-step approach:

- I. Literature review about the pulmonary drug delivery systems, DPIs, synthesis of polymer, nanotechnology to develop the INH loaded DPIs and QbD approach along with DoE in developing the optimized DPIs.
- II. Use of different polymers such as chitosan (CS) and mannosylated chitosan (MC) along with hyaluronic acid (HA) to design the different hybrid INH loaded nanopowders to target the AM in lungs for the effective treatment of TB.
- III. Application of the cost-effective ionic gelation method for the preparation of nanosuspensions for further spray-drying or freeze-drying. Selecting different concentrations of the polymers and drug to design different runs following the initial risk assessment and DoE to optimize the nanopowders.
- IV. Structural and morphological examination of the developed nanosystems along with physicochemical characterization through different *in vitro* techniques. Moreover, the *in silico* studies were also performed to evaluate the deposition profile of nanopowders in the lungs.
- V. *Ex vivo* studies on the different cell lines to demonstrate the behaviour of nanopowders in terms of toxicity, immune-regulation, and tolerogenic effects, particularly on human-derived macrophages.

3. LITERATURE BACKGROUND

3.1 Pharmaceutical and immunological aspects

3.1.1 Pathogenesis of Tuberculosis

The bacterial pathogen, M.Tb, is the cause of millions of death across the globe. The bacteria enter the human body via the inhalation pathway. Once inside the human body, M.Tb gets into the interstitium of the lungs and spreads to the different organs in case of a chronic condition. After the invasion of bacteria in the other parts of the body, the immune-compromised patients are unable to survive in the majority of the cases [4]. The immune cells of the body initiate the pro-inflammatory response to minimize the damage to the pleural tissues. AM functions as a niche for the survival and replication of the bacteria in TB. M.Tb survives on the lipid droplets inside AM and forces the AM to produce and store the lipid droplets. Besides, the glycolic metabolic pathway is compromised and leads to the development of foamy macrophage (granuloma), which is the containment of immune cells including lymphocytes, macrophages, infiltrated monocytes, Langerhans cells, and epithelioid cells [5]. Granuloma might lead to localized necrosis and releases the bacteria through airways in the chronic condition, making the subject a carrier and cause of the further spread of TB [6].

To maintain the innate immune defence of the body, macrophages play a key role. Macrophages identify and phagocytose the M.Tb that bears the pathogen-associated molecular patterns (PAMPs) through membrane-associated pattern recognition receptors (PRRs). This interaction initiates the cascade of pro-inflammatory responses by the production of pro-inflammatory cytokines such as interleukin-12, interleukin-1 β , and tumour necrotic factor- α (TNF- α) [7]. Likewise, the T-cell response in adaptive immunity is crucial as it counterbalances the pro-inflammatory but protective response by Th1 cells. Suppression of T-cell response can be detrimental to the patient as it may stimulate the cascade of events towards an anti-inflammatory response which is not favourable in resolving TB and cause resistance again TB [8]. AM are stimulated towards the T-cell response and hence can be targeted in the TB to regulate the immune response. Moreover, AM targeting can be exploited to eradicate the bacterial load and hence the treatment of disease at a cellular level.

3.1.2 Limitations to the treatment of Tuberculosis

Currently, available marketed dosage forms (Table 1) have failed to treat TB effectively. The conventional treatment regimen is based on the combination of bacteriostatic and bactericidal

drugs and takes over 6 months following the standard course of therapy which comprises first-line anti-tubercular drugs (isoniazid, rifampicin, pyrazinamide, and ethambutol) along with streptomycin. However, it takes up to 2 years of chemotherapy with second-line drugs such as aminoglycosides and fluoroquinolones in the patients who develop multiple-drug resistant TB due to prolonged drug intake [9]. As the orally administered drugs have to undergo the first-pass metabolism in the liver, therefore not only poses hepatotoxicity but also leads to the inadequate availability of the drug at the pathological target site. Moreover, the prolonged duration of therapy is also associated with the potential compromise to the normal functioning of the liver and kidneys. With the emergence of the new strains of TB, it is becoming difficult to treat the disease at the cellular level of infection following the conventional drug delivery routes that fail to deliver anti-tubercular drugs to the lung lesions. Another barrier to the clinical management of TB is the poorly vascularized lung lesion that is fortified with thick fibrous tissue. Therefore, the parenterally administered dosage forms are also unable to bypass this barrier efficiently [10]. All these limitations lead to the incomplete eradication of bacterial load from the granulomas resulting in the dormant or inactive latent infection. Upon activation, the M.Tb can spread into the peripheral lymph nodes, brain, gastrointestinal tract, and skeletal muscles developing the secondary TB lesions (requiring surgical intervention in most cases) that become life-threatening if left untreated [11]. Also, the economic crises in the low and middle-income countries leave a gap in achieving the global TB eradication target. According to the statistics reported by the UN high-level TB meeting in 2020, an annual grant of US\$ 13 billion is required to prevent, diagnose and treat TB globally.

Table 1: Currently available marketed dosage forms for the therapy of TB

	Drug	Effect	Target	Mechanism of action	Marketed dosage form and adult dose
Fist-line drugs	Isoniazid	Bactericidal	Acyl carrier protein reductase	Inhibition of bacterial cell wall mycolic acid synthesis and disruption of metabolic pathway	<i>Tablets:</i> 300 mg once a day, or up to 900 mg twice a week. <i>Injection:</i> 5 mg/kg up to 300 mg single dose daily.
	Rifampicin	Bactericidal	RNA polymerase subunits	Inhibition of RNA synthesis	<i>Capsule:</i> 10 mg/kg/day <i>Powder for injection:</i> 600 mg/day for prophylaxis
	Pyrazinamide	Bacteriostatic/ Bactericidal	Membrane and metabolism channel	Dysregulation and disruption of bacterial membrane transport channels and energy depletion	<i>Tablet:</i> 500 mg once a day not exceeding 2 g/day
	Ethambutol	Bacteriostatic	Arabinosyl transferase	Inhibition of arabinogalactan synthesis in cell wall	<i>Tablet:</i> 25 mg/kg daily, not exceeding 2 g/day
	Streptomycin	Bactericidal	Ribosomal protein and 16S rRNA	Inhibition of protein synthesis	<i>Powder for injection:</i> 15 mg/kg IM, no more than 2 g/day
Second-line drugs	Levofloxacin	Bactericidal	DNA gyrase	Inhibition of DNA synthesis	<i>Tablet:</i> 10 mg/kg daily not exceeding 1 g/day
	Ethionamide	Bacteriostatic	Acyl carrier protein reductase	Inhibition of bacterial cell wall mycolic acid synthesis	<i>Tablet:</i> 250 mg daily, not more than 1 g/day
	Kanamycin	Bactericidal	16S rRNA	Inhibition of protein synthesis	<i>Injectable solution:</i> 15 mg/kg/day by IV or IM route. <i>Aerosol:</i> 250 mg twice a day by nebulization
	Cycloserine	Bacteriostatic	D-alanine racemase	Inhibition of peptidoglycan synthesis	<i>Capsule:</i> 500 mg/day not more than 1 g/day

3.1.3 Various pulmonary drug delivery mechanisms using different devices

Different types of aerosol-based devices are currently available in the market for the delivery of drugs to the lungs. The use of an effective technique determines the adequate therapeutic

dose for the lungs. Recently, nebulizers, pressurized meter dose inhalers (pMDIs), and dry powder inhalers (DPIs) are the widely explored techniques for inhalation (Table 2). Nebulizers have been exploited in the past for the treatment of chronic diseases such as asthma and chronic obstructive pulmonary disease (COPD). The air flow in the nebulizer converts the medicine into a mist for inhalation. Nebulizers allow administration of large doses and are most commonly used for bed-compromised patients. However, only 10 % of the dose can reach the lungs. Also, the limitations of stability and solubility of the formulations for nebulization exist. Due to these reasons, nebulization of a large volume of highly concentrated suspension might result in the precipitation of particles [12]. Another drug delivery approach for COPD is the pMDI. This technique uses propellants to deliver the drug to the lungs and is limited by the fraction of the dose that can be delivered in a single puff. Recently, chlorofluorocarbons have been replaced by hydrofluoroalkane propellant due to safety concerns. The drug deposition profile equivalent to 50 % can be achieved via this technique. However, despite being economical and easy to handle, pMDIs have certain limitations such as high pharyngeal deposition and an upper limit to unit dose content [13]. Due to the drawbacks of low drug deposition and complex manufacturing, the mentioned techniques are unfavourable for TB therapy. To overcome this issue, DPIs have gained interest over time. DPIs are easy to manufacture with reconstituted powder without the need for cold storage [14].

Moreover, DPIs are propellant-free, patient-friendly, and can be used for single and multi-dose administration. A high drug deposition can be achieved leading to higher availability of the drug at the target site in TB [15-18]. DPIs can be exploited for systemic and local drug delivery, their performance is however dependent on the powder parameters and device characteristics. Moreover, the particles of less than 5 μm are optimal for pulmonary drug delivery by DPIs [19]. Since the invention of the Spinhaler[®] device, there has been an advancement in the DPIs manufacturing technology and thus a variety of DPIs devices are available in the market now. Nonetheless, there are certain limitations related to the powder agglomeration that can be rectified by improving the particle engineering methods.

Table 2: Various pulmonary aerosol devices on the market

Devices	Properties	Mechanism	Commercial brands	Exploited areas
Nebulizer	Drug solution and suspension-based compositions, not useful for thermolabile compounds	Venturi's principle, work with fluid pressure	Akita [®] jet eFlow [®] Aeroneb [®] Go	Asthma, COPD, Lung infections
Pressurized metered-dose inhalers (pMDI)	Drug solution and suspension aerosolization	Propellant based breath-actuated device	Respimat [®] Aerochamber [®]	Asthma, COPD, Smoking cessation, Lung infections
Dry powder inhalers (DPIs)	Portable small devices, easy administration, dry powders composition	Passive breath actuate device without any propellant	Aerolizer [®] Flexhaler [®] Breezhaler [®] Ellipta [™]	COPD, Hypertension, TB, Asthma, Lung infections Bronchitis

3.1.4 Nanotechnology as a new paradigm in pulmonary drug delivery

Due to the obstacles, associated with the non-targeted approaches, such as low drug bioavailability, low drug stability, inadequate availability of the drug at a target site, and high drug degradation following hepatic metabolism, it is thereof favourable to use the recent advancement in science, i.e., nanotechnology. The advent of nanotechnology has brought about a revolution in the therapeutics and diagnostics of infectious diseases. The use of engineered nanoparticles (NPs) with at least one dimension in the nanoscale range (<1 μm) can improve the drug delivery approach in TB. NPs exhibit high colloidal stability, enhanced bioavailability, less toxicity, improved drug release profile, and minimal off-site drug accumulation [20]. Various types of nanostructures are being developed and studied for their application in nanotherapeutics. The versatility in the composition exists because of the difference in the surface chemistry, physicochemical parameters, sensitivity, and specificity aimed at different body organs using different routes of administration. Over a decade, the improvement in nanotechnology has offered improved pharmacokinetics and therapeutic efficiency in the management of pulmonary TB. The pulmonary route of administration is an emerging and currently most exploited field of nanomedicine for antibiotics delivery. The pulmonary route retains many advantages such as higher drug deposition in the deeper areas of the lungs, an

extensive alveolar network for the absorption of the drug, avoidance of the first-pass effect, and engulfment of particles by the AM [21]. Direct administration of the drug to the lungs is an alternative yet promising strategy as it facilitates the drug availability at the target site with less systemic exposure. The localized delivery of anti-tubercular in TB can help in the inhibition of the infection from the lungs before it traverses to the secondary organs.

Moreover, the adequate availability of the anti-tubercular at the target site in the lungs can reduce the dosage frequency and reduce the chances of drug resistance in M.Tb, thereby improving patient adherence. DPIs and pressurized metered-dose inhalers (pMDIs) are the most commonly investigated non-invasive methods to deliver drugs to the lungs [17]. DPIs are the pulmonary drug delivery systems with dispersible particles with high drug load and stability. They possess high physicochemical stability as compared to liquid inhalers. Moreover, they are handy, environment-friendly, and affordable. Also, the DPIs do not require the propellants for aerosolization but are rather breath-actuated.

Previously, the microparticles-based DPIs have been investigated which have shown promising outcomes. DPI based on the microparticulate anti-tubercular capreomycin is under clinical trial, which demonstrated that the inhaled TB therapy improves the treatment regimen [22]. Moreover, the patent (US20070128124A1) also exists which evaluates the pharmacokinetic behavior of the aerosolized capreomycin DPI. Presently, the use of nanotechnology has been taken into consideration to develop the DPIs, Table 3.

DPIs comprised of NPs have improved aerodynamic profile, enhanced deposition in the deeper areas of the lungs, and have a high drug payload [23]. Using nano-DPIs combine the advantages of nanoscale particles and aerosols in one formulation to achieve a higher localized effect, increased alveolar uptake, improved pharmacokinetics, and extended release of a drug.

To achieve the higher deposition of nanopowders by inhalation, parameters such as mass median aerodynamic diameter (MMAD) and fine particle fraction (FPF) must be taken into account. MMAD is defined as the cut-off diameter of the particles at which 50 % of the particles are smaller or larger by mass deposited in the lungs, whereas $FPF < 5 \mu\text{m}$ and $FPF < 3 \mu\text{m}$ defines the particles to be deposited in the bronchial region and the deeper lung tissues respectively [24].

Table 3: Most commonly exploited nanotechnology-based anti-tubercular dry powders for inhalation

Delivery system	Composition	Encapsulated moiety	Synthetic approach	Reference
Self-assembled polymeric NPs	Poly(lactide-co-glycolide) PLGA	Rifampicin	Solvent evaporation and spray-drying	[25]
Solid lipid NPs	Glyceryl tri-stearate and glyceryl dibehenate	Rifabutin	Hot high shear homogenization and spray-drying	[26]
Polymeric NPs	Chitosan	Bedaquiline	Ionic gelation and freeze-drying	[27]
Nanocluster metal dendrimers	Methylmethacrylate, copper sulfate, and ethylenediamine	Isoniazid	Template synthetic approach and evaporation	[28]
Niosomes	Cholesterol, Tween-80, Tween-20, Span-60, Span-80 and Span-20	D-cycloserine and ethionamide	Ethanol injection followed by solvent evaporation	[29]
Polymeric micelles	Poly (vinyl caprolactam)-poly (vinyl acetate)-poly (ethylene glycol)	Rifampicin	Solvent diffusion and evaporation	[30]

3.1.5 Polymeric nanoparticles for the delivery of anti-tubercular drugs

Polymers are the macromolecules made up of the linkage of monomers via the functional groups, in a linear branched structure. Different polymers can be constructed to attain the desirable features which make them highly versatile materials in nanomedicine. The salient features of using the polymers as drug delivery vehicles are biodegradability, improved retention time, biocompatibility, sustained or controlled drug release, and site-specific targeting [31]. Tailoring of the polymer by derivatization can also be done to obtain the particular properties. Here, we have explored the potential of polymer-based (chitosan and mannosylated chitosan, hyaluronic acid) nanotherapeutics due to high stability, improved circulation, biodegradability, biocompatibility, improved retention in the pulmonary tissues, and suitable surface chemistry [32]. Besides, both the hydrophilic and lipophilic drug moieties can be encapsulated in polymeric nanostructures. Likewise, the targeted polymeric NPs can retain a high drug load, which ultimately reduces the off-site dose-dependent toxicity on the various organs. Polymeric NPs loaded with antimicrobials can circumvent the mucosal and cellular barriers to localize the drug to the target organ. Based on the research rationale, biodegradable

polymers were selected for designing the nanoplexes for pulmonary administration of anti-tubercular.

3.1.5.1 Chitosan and its derivatives

Chitosan is a polysaccharide of marine origin with β -(1 \rightarrow 4)-linked 2-acetamido-2-deoxy- β -D-glucopyranose and 2-amino-2-deoxy- β -D-glucopyranose [33]. The polymer is a weak base and is soluble in dilute aqueous acids. Because of its marine crustacean origin, it is biocompatible and biodegradable. These features are essential to the development of biocompatible nanoplexes for drug delivery. Moreover, the presence of primary amino groups in CS is responsible for its transfection and mucoadhesion. Due to its antibacterial properties, FDA has approved the use of CS as wound dressings. The use of CS in the pulmonary drug delivery system allows the retention of NPs in the epithelial mucosa for a long duration which can be attributed to the formation of a hydrogen bond between the glycoprotein in the mucous and, the carboxyl and amino groups of CS. Also, CS allows the paracellular absorption of the drug in the pulmonary epithelia. It has been established that CS, due to its cationic nature, stimulated the pro-inflammatory response in the lungs in a dose-dependent manner [34], which was the intended outcome of our research. All these qualities make CS a favourable polymer for the pulmonary route of drug delivery. Similarly, another widely employed polymer derivative of CS is the mannose conjugated chitosan, i.e., mannosylated chitosan (MC). It is a non-toxic linear polysaccharide comprised of repeating N-acetyl-D-glucosamine and D-glucosamine units [35]. The surface of AMs overexpresses (CD206) mannose receptors during pathogenic infections and inflammation. The mannose receptors can recognize the pathogens' mannose and fucose moieties via their pattern recognition domains. Moreover, M.Tb activates the mannose receptor on alveolar macrophages and hence plays a pivotal role in the pathogenesis of TB. Similarly, this idea can be utilized to target the mannose receptors on macrophages by utilizing the MC as a carrier for drug delivery in TB. In this way, the macrophages can efficiently engulf the NPs due to mannose composition.

3.1.5.2 Hyaluronic acid

Besides, hyaluronic acid (HA) was also employed in this work. HA is also a polysaccharide from a natural origin that is composed of repeating units of β -glucuronic acid and N-acetyl-D-glucosamine. Due to its characteristics such as biodegradation and biocompatibility, HA poses no toxicity to the pulmonary cells [36]. Additionally, HA protects the lungs against pleural

thickening and epithelial injury in TB without eliciting an allergic response [37]. Also, HA improves the mucociliary transport in pulmonary tissues and affects the inflammatory mediators in the lungs as well as the agglutination of AM [38]. Furthermore, CD44 receptors on the activated macrophages recognize the HA and facilitate the adhesion of NPs to the surface of AM therefore, CD44 receptors can be explored as targets in the targeted drug delivery to AM in TB.

3.1.6 Drying methods to obtain DPIs

3.1.6.1 Methods for developing DPIs by freeze-drying

Several techniques are used to obtain the dry powders following the fabrication of nanosuspensions. However, the drying techniques are selected based on the physicochemical properties of the sample. Numerous studies have demonstrated the effectiveness of lyophilization or freeze-drying to remove the liquid phase from samples to acquire dry powder. The temperature of the process may be varied at different stages, from -40 °C to -5 °C. The primary drying step removes solvent by subliming the frozen water and the second step eliminates unfrozen water. Throughout the process, vacuum is applied and conduction is responsible for providing the sublimation energy to the samples. The freeze-drying time increases as the product sample height increases [39]. Cryoprotectants such as trehalose, a disaccharide, are often used in freeze-drying to obtain powders with high stability. Moreover, the redispersion of the samples can also be improved by using trehalose. Freeze-drying improves the aerosolization of the particles. The primary goal of the drying process is to improve the stability of the samples. In this process, elevated temperatures are not required for drying, a homogeneous dispersion is obtained and is highly recommended for the samples sensitive to air. The acquired dry powders have an elegant outlook with a cake appearance. FDA has approved the freeze-drying technique to obtain the inhaled biologics dry powder [40]. In 2014, FDA approved the dry insulin powder for inhalation (Afrezza[®]) which employed freeze-drying in its manufacturing. On the other hand, few disadvantages do exist for this method, such as the use of mechanical stress as post-process to reduce the particle size of dried powders, which often get agglomerated. Also, the scale-up setup is expensive, time-consuming, and is a multi-step procedure [41].

3.1.6.2 Methods for developing DPIs by spray-drying

Spray-drying is the most well-established technique for obtaining dry powders. The use of spray-drying dates back to the 20th century when it was used for drying blood [42]. It is applied widely to obtain pharmaceutical powders with multiple size ranges. The use of spray-drying in the pulmonary drug delivery powders is being explored vastly as the process allows the control over the parameters that can affect the size distribution, density, morphology, and dispersibility. The method generates solid particles in a single-step process. The process involves atomization, drying, and separation of powder altogether in one step. Atomization results in the spraying of liquid feed through the nozzles forming droplets. The droplets are dehydrated due to heating in the drying chamber and the resulting dry powder is collected in the collecting chamber. For colloidal systems, the size of the nozzle orifice should be larger than the size of the dispersed feed. Also, the low feed concentration yields powders with small aerodynamic diameters and homogenous size distribution [43]. The commercially available DPIs use α -lactose monohydrate as a carrier for spray-drying. The excipient has been developed industrially into a high-quality crystalline InhaLac[®] 400 (I400) to meet the requirements for the DPIs. I400 not only improves the powder handling but also the performance efficiency of the inhaler [44]. However, I400 might become amorphous during spray-drying which might impart hygroscopicity to the dried product. Unlike I400, mannitol is not of animal origin and does not contain the reducing functional groups. Moreover, it imparts crystalline properties to the yielded dry powder. The surface morphology can be changed by using mannitol at different concentrations at different outlet temperatures [45]. Mannitol has also been approved in the EU for the add-on therapy in patients with cystic fibrosis [46]. It is also demonstrated to increase the osmotic pressure of the fluid around the mucosal epithelia in the lungs that helps in the clearance of mucous in cough with phlegmy by reducing mucosal viscosity [47]. Inlet temperature, outlet temperature, flow rate, and peristaltic feed pump velocity can be altered during the spray-drying depending on the composition of samples. To obtain the nano-dimensional particles, nano-spray dryers are utilized.

3.2 Regulatory aspects

3.2.1 Quality by Design approach

Quality by Design (QbD) is a systematic robust approach to understand the relationship between product attributes and product performance.

The main goals of the systematic time-saving approach to determine the pre-defined objectives are:

- a) to obtain the product with defined specifications for meaningful clinical performance,
- b) to minimize the product variability by optimizing the product and process design and control,
- c) to efficiently improve the material and process attributes to get a high-performance product,
- d) to facilitate the post-approval challenges and management of post-marketing surveillance.

This holistic process has been established by the International Council for Harmonization of Technical Requirements for Pharmaceuticals for Human Use (ICH) and mentioned in international guidelines [48-50]. Furthermore, FDA introduced QbD in the development of pharmaceutical products from conceptualization to commercialization. Conventionally, the pharmaceutical product is developed and tested for quality controls through rigorous testing and if the product complies with the standard quality specifications, then it is considered fit for commercialization. This whole-time-taking task might have to be reprocessed in case of failure. QbD, on the other hand, involves multivariant experiments to identify the objectives and determine the outcomes without compromising the quality of the end product [51].

The approach begins with knowledge space development which is defined as the organized collection of literature. After a thorough investigation of published data, the quality target product profile (QTPP) is defined depending on the requirements of the clinicians, patients, and industry. The criterion for establishing the QTPPs are described in ICH Q8 (R2) guidelines [52]. Afterward, the critical quality attributes (CQAs) are determined. The CQAs are the factors that influence the physical, chemical, biological, and morphological characteristics of the product. Similarly, critical material attributes (CMAs) and critical process parameters (CPPs) are shortlisted, which are the material and process features impacting the final product quality. Following, the risk assessment is performed by analyzing the interdependence between QTPPs and CQAs and, CQAs and CPPs/CMAs on the 3-grade scale of low (L), medium (M), and high (H). To check this interdependency, Lean QBD software[®] (QBD works LLC, Fremont, USA) was used in this work.

3.2.2 Design of Experiment (DoE)

Design of Experiment (DoE) assists in understanding the attributes influencing the investigated process. DoE has numerous advantages such as studying the various factors at the same time by determining the interaction between them. The experimental limitations are also taken into account in DoE which is not possible with traditional experimental designs [53]. The traditional formulation and product development is a time-consuming task. On the contrary, DoE is a cost-effective and proficient approach for assessing the critical factors, determined during the risk assessment, in further screening design. The designs may vary according to the number of dependent and independent variables.

Here, the Box-Behnken design was employed to study the correlation between the parameters and their influence on the dependent attributes [54]. The design gave the minimum number of experimental trials with high precision outcomes.

4. MATERIALS AND METHODS

4.1 Materials

Isoniazid was purchased from Pannon Pharma Kft (Hungary). Chitosan [75–85 % deacetylated, low molecular weight, 50-190 kDa, Poly (D-glucosamine)] and 4',6-diamidino-2-phenylindole (DAPI) dye, trehalose and dialysis membrane (12000–14,000 Mw cut-off) were obtained from Sigma-Aldrich (MO, USA), whereas 3-(4,5-dimethylthiazol-2-yl)-2,5 diphenyltetrazolium bromide (MTT), D-mannose, 4-Dimethylamino benzaldehyde (Ehrlich's reagent), hydroxylamine chloride and sodium dodecyl sulfate (SDS) from Sigma-Aldrich Chemie GmbH, (Steinheim, Germany).

Sodium hyaluronate equivalent to $1.5-1.8 \times 10^6$ Da (Hyaluronic acid) was provided by Contipro Biotech (Czech Republic). Sodium tri-polyphosphate was purchased from Alfa Aesar (ThermoFischer, Germany). Mannitol and InhaLac[®] 400 were provided by MEGGLE Group, (Wasserburg, Germany). Glacial acetic acid was purchased from Molar Chemicals Kft. (Hungary).

Macrophage Raw 264.7 and A549 cell lines were purchased from ATCC (VA, USA). 3-(4,5-dimethylthiazol-2-yl)-5-(3-carboxymethoxyphenyl)-2-(4-sulfophenyl)-2H-tetrazolium (MTS) cell proliferation assay kit was purchased from BioVision (CA, USA). EDAC (1-ethyl-3-(3-dimethylamino propyl) carbodiimide hydrochloride) and thioglycolic acid from Tokyo Chemical Industry Co., Ltd. (Japan). PSG (100 u/ml penicillin, 0.1 mg/ml streptomycin, and 2 mM L-glutamine and Fetal Bovine Serum (FBS) were purchased from Invitrogen (CA, USA).

Roswell Park Memorial Institute medium (RPMI-1640) Dulbecco's modified Eagle's medium (DMEM) were bought from GIBCO® (ThermoFischer Scientific, MA, USA). Ficoll-Paque TM PLUS (density 1.077 g/ml) was purchased from GE Healthcare Bioscience AB (IL, USA). Trifluoroacetic acid was from Merck Schuchard OHG, (Hohenbrunn, Germany).

Phycoerythrin (PE)-conjugated anti-human CD80 (CD80-PE), Granulocyte-macrophage colony-stimulating factor (GM-CSF), and Allophycocyanin (APC)-conjugated anti-human CD83 (CD83-APC) were obtained from Miltenyi Biotec (Bergisch Gladbach, Germany). Sterile and autoclaved materials were used for *in vitro* experiments. All the chemicals used were of high purity or reagent grade.

Table 4: Properties of the active ingredient, Isoniazid

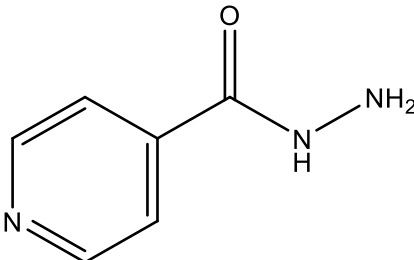
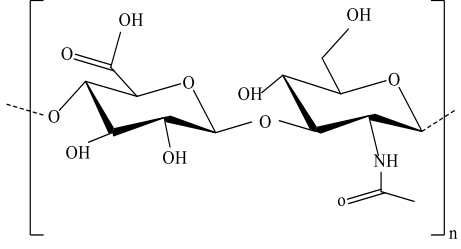
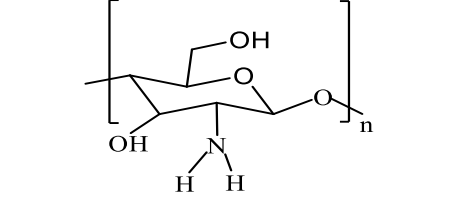
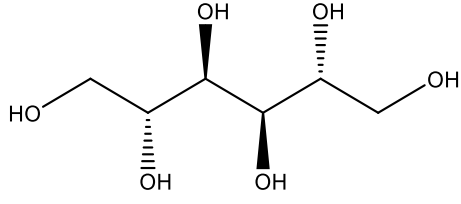
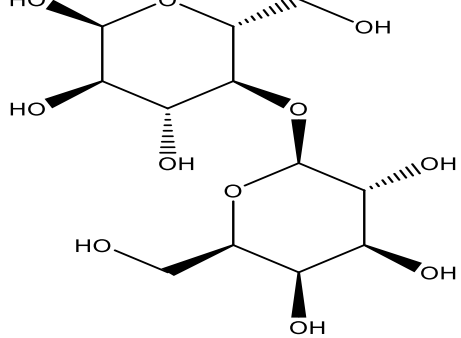
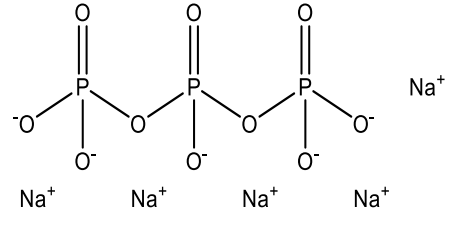
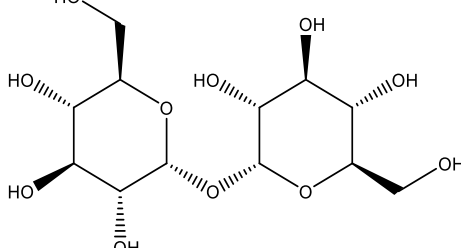
Structure	
Chemical name	Isonicotinylhydrazide Pyridine-4-carbohydrazide
Molecular weight	137.139 g mol ⁻¹
Melting point	171.4 °C
PKa	1.82
Physical properties	White odourless crystalline powder. Soluble in alcohol at 25 °C, partial solubility in water (14 %)
Toxicity concerns	Liver damage, central nervous system toxicity, acute oral toxicity, reproductive toxicity, metabolic acidosis, loss of appetite and jaundice. All these adverse effects are dose-dependent.
Mechanism of action	Bactericidal when Mycobacteria grows rapidly and bacteriostatic when Mycobacteria replicates slowly. It inhibits mycolic acid synthesis in Mycobacteria and interferes with cell wall synthesis to produce bactericidal activity. For bacteriostatic effect, it suppresses bacterial growth at the log phase.
Marketed dosage forms	Oral (liquid): 50 mg/5 ml Oral (solid): 50 mg tablet 100 mg tablet 300 mg tablet Parenteral (IV): 100 mg/ml

Table 5: Properties of additives and excipients

Compound	Chemical structure	Physical properties	Role
Hyaluronic acid	 <p>The structure shows a repeating unit of a disaccharide chain. It consists of a D-glucuronic acid unit linked to a 3-O-acetyl-D-glucosamine unit. The units are connected by a beta-1,3-glycosidic bond. The glucuronic acid unit has hydroxyl groups at C2, C3, and C4, and a carboxylic acid group at C5. The glucosamine unit has a hydroxyl group at C2, a hydroxyl group at C3, and an acetamido group at C2. The chain is enclosed in brackets with a subscript 'n'.</p>	<p>M_w: $1.5-1.8 \times 10^6$ Da</p> <p><i>Solubility</i>: in water</p>	<p>Polymer</p> <p>Shell component</p>
Chitosan	 <p>The structure shows a repeating unit of a poly(N-acetylglucosamine) chain. It consists of a D-glucosamine unit with an acetamido group at C2. The units are connected by a beta-1,4-glycosidic bond. The structure is enclosed in brackets with a subscript 'n'.</p>	<p>M_w: 50-190 kDa</p> <p><i>Solubility</i>: in dilute aqueous acidic acid</p>	<p>Polymer</p> <p>Shell component</p>
Mannitol	 <p>The structure shows the open-chain form of mannitol, a six-carbon polyol. The hydroxyl groups are at C2, C3, C4, and C5. The hydroxyl groups at C2 and C4 are on the same side (wedges), while the hydroxyl groups at C3 and C5 are on opposite sides (one wedge, one dash).</p>	<p>M_w: 180.2 g/mol</p> <p><i>Solubility</i>: in water and alcohol</p>	<p>Diluent</p> <p>Bulking agent</p>
InhaLac [®] 400	 <p>The structure shows a disaccharide unit of InhaLac 400, which is a mixture of alpha-D-glucopyranose and beta-D-fructofuranose. The two units are linked by a beta-1,2-glycosidic bond. The glucose unit has hydroxyl groups at C2, C3, C4, and C6. The fructose unit has hydroxyl groups at C2, C3, C4, and C5.</p>	<p>M_w: 342.3 g/mol</p> <p><i>Solubility</i>: in water, ethanol, and methanol</p>	<p>Diluent</p> <p>Bulking agent</p>
Sodium tri-polyphosphate	 <p>The structure shows a linear chain of three phosphate groups linked by phosphoanhydride bonds. Each phosphate group is bonded to a sodium ion (Na+). The structure is shown as a chain of three phosphate groups with four sodium ions associated with them.</p>	<p>M_w: 367.8 g/mol</p> <p><i>Solubility</i>: in water</p>	<p>Cross-linker</p>
Trehalose	 <p>The structure shows a disaccharide unit of trehalose, which is 4-O-alpha-D-glucopyranosyl-D-glucopyranose. The two glucose units are linked by an alpha-1,4-glycosidic bond. Both units have hydroxyl groups at C2, C3, C4, and C6.</p>	<p>M_w: 342.2 g/mol</p> <p><i>Solubility</i>: in water</p>	<p>Cryoprotectant</p>

4.2 Method

4.2.1 Synthesis of polymer

The CS polymer was modified by using the previously reported method [55]. Briefly, thioglycolic acid (TGA) was poured into the 1 % CS solution in acetic acid. After subsequent addition of 50 mM EDAC (1-ethyl-3-(3-dimethylamino propyl) carbodiimide hydrochloride)) to activate carboxylic groups of TGA, an amide linkage between CS and TGA developed. The obtained polymeric suspension, thiolated chitosan (TC), was dialyzed using a dialysis membrane (molecular weight cut-off 12–14 kDa) against double distilled water for 3 days to remove the unbound TGA. After freeze-drying, amorphous polymeric mass was obtained. Later, MC was synthesized by the conjugation of D-mannose to the TC. For this purpose, 0.12 M cyanoborohydride was added to the 2 % TC suspension (solubilized in acetic acid) to facilitate the reductive amination (Figure 1). Following, 0.33 M D-mannose was added to the suspension with continuous stirring. The pink polymeric suspension of MC was acquired which was dialyzed against methanol four times and with double distilled water once. The resulting final product was freeze-dried and kept in a light-resistant and air-tight container.

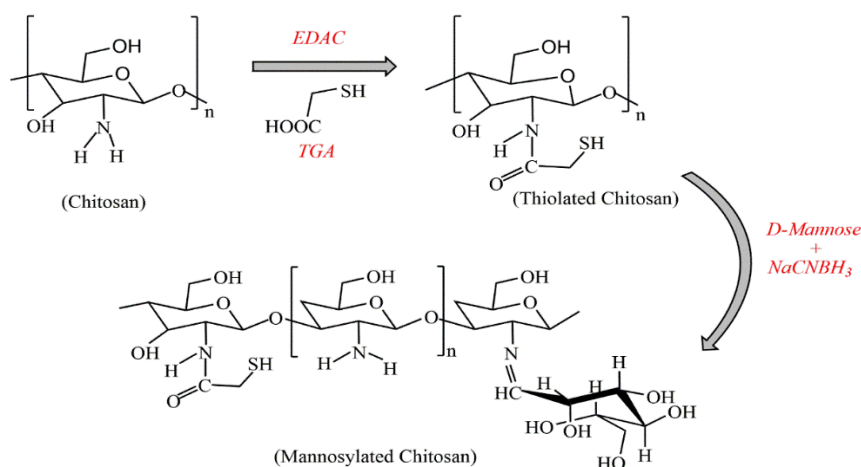


Figure 1: The schematic pathway for the synthesis of mannosylated chitosan. Thiol anchorage to chitosan is mediated through amide bond formation between the amino group of chitosan and the carboxyl group of thioglycolic acid. Following, the anchorage of mannose to the thiolated chitosan via Schiff's base ($R-CH=N-R$) mediated amide linkage between the aldehyde group of D-mannose and amino group of thiolated chitosan.

4.2.2 Quantification of polymer

First, the bound thiol groups to MC were quantified against the TGA standard. The polymer was solubilized in deionized water in individual experiments and 5 ml phosphate buffer (pH 8)

was added along with 0.5 ml Ellman's reagent. The solution was centrifuged at 23,500 g for 10 min and the obtained supernatant was analyzed at 430 nm using a microplate reader (Perkin Elmer) [56]. Furthermore, the number of disulfide bonds was also quantified by determining the number of free thiol groups. For this quantification, the free thiol groups were subtracted from the total thiol groups attached to the MC polymer [57]. The polymer was dissolved in deionized water separately, phosphate buffer (pH 6.8) was added and 1 ml sodium borohydride was infused dropwise followed by an incubation period of 2 h. Later, 100 μ l of 5 M HCl was added to remove the excess sodium borohydride. The suspension was again incubated for 1 h after the addition of 0.1 ml Elman's reagent. The samples were poured into a 96-well plate and optical density (OD) was recorded using a microplate titration reader. Likewise, mannose groups were quantified on the MC by hydrating the polymer in deionized water in a 96-well plate. 50 μ l of pristine (2,6,10,14-tetramethyl-pentadecane), 100 μ l of sulfuric acid, and 20 μ l of resorcinol were added. The well plate was kept in an oven at 90 °C for 30 min. the OD was analyzed at 450 nm using a microplate reader.

4.2.3 Characterization of polymer

For the characterization of synthesized polymer MC, ^1H NMR spectroscopy (Bruker BRX-500) was performed. For this purpose, the polymer was solubilized in deuterated DMSO for the analysis. CS spectra were also recorded for comparison.

4.2.4 Application of QbD

4.2.4.1 Knowledge space development and defining quality target product profile (QTPP)

The term, "knowledge space development" encompasses the collection of previously published scientific data organized systematically. After thorough data collection and study, QTPPs were chosen based on the requirements of the clinicians, patients, and industrialists. Moreover, the detailed approach to the consideration of QTPP is described in ICH Q8 (R2) guidelines [52].

4.2.4.2 Determining CQAs, CPPs, and CMAs

CQAs are defined as the factors which forecast pronounced effects on the QTPP. The factors encompass the physical, chemical, biological or morphological characteristics that should be considered during the development of formulation. The outcome of these CQAs also functions to affect the therapeutic aims. Similarly, CMAs and CPPs were scrutinized based on knowledge space development. CMAs and CPPs are the critical material and process attributes that directly influence the CQAs.

4.2.4.3 Initial risk assessment

The interdependence between QTPPs and CQAs, and between CQAs and CMAs/ CPPs was assessed following the scrutiny of the critical attributes. This interdependence was based on the 3-grade scale of low (L), medium (M), and high (H). For this purpose, Lean QBD software[®] (QBD works LLC, Fremont, USA). The attributes were ranked in the order of their impact which was shown by the software as Pareto charts that further assisted in the factorial design of the experiments.

4.2.5 Design of Experiment

Pharmaceutical product development through conventional design is a cumbersome process. On the contrary, DoE is an efficient and robust method to evaluate the critical factors and steps of formulation development [58]. The variables for the screening DoE were selected based on risk assessment. For this Ph.D. work, Box-Behnken (BB) was chosen to take into consideration the various variables simultaneously to save time and resources. BB is the common way to study the relationship between critical factors and their influence on the aimed attributes. Furthermore, BB gives the lowest number of experimental runs with high accuracy. The effect on the response variables was studied against the identified highest critical factors defined through risk assessment. The independent factors chosen through risk assessment were the concentration of HA (X_1 , lower limit: 2.5 mg, upper limit 6.5 mg), the concentration of CS (X_2 , lower limit: 1.25 mg, upper limit 3.25 mg), and sonication pulse ratio (X_3 , lower limit: 30, upper limit 50). On the other hand, 3 dependent or response variables were selected (Y_1 : size, Y_2 : polydispersity index (PDI), Y_3 : zeta potential). A set of experimental runs was generated by STATISTICA[®] 10 software that used ANOVA for statistical significance ($p < 0.05$). The established polynomial model (equation 1) was obtained after the regression analysis of each response, which is as followed,

$$Y = \beta_0 + \beta_1 X_1 + \beta_2 X_2 + \beta_3 X_3 + \beta_{12} X_1 X_2 + \beta_{13} X_1 X_3 + \beta_{23} X_2 X_3 + \beta_{11} X_1^2 + \beta_{22} X_2^2 + \beta_{33} X_3^2 \quad [1]$$

Where Y is the response, X_1 - X_3 are the main effects of factors, $X_1 X_2$, $X_1 X_3$, and $X_2 X_3$ are the interaction factors. β_0 is the constant and β_1 - β_3 are the coefficients of factors.

4.2.6 Preparation of nanosuspensions

An ionic gelation method was employed to develop the NPs by using cross-linker sodium tri-polyphosphate (TPP). Polymer, CS was solubilized in 0.5 M Glacial acetic acid. The pH of the polymeric system was maintained at 4.9. Similarly, HA was dissolved in double distilled water

to obtain a polymeric suspension. Based on experimental runs acquired from the DoE setup, different concentrations of the polymers were used. TPP (0.5-2 mg/ml) was added dropwise to the CS suspension until the appearance of a bluish haze followed by the addition of HA suspension under probe sonicator. The interaction between the cationic surface groups of polymers and negative surface groups of TPP creates NPs with a plexus network. Using this approach, a drug can be encapsulated after the fabrication of NPs. Later, 10 mg of INH (10 % of oral dose) solubilized in 1 ml methanol was injected into the prepared nanosuspension to obtain INH loaded CS and HA NPs (INH-CS/HA NPs). Organic solvent was then evaporated by overnight stirring to encapsulate maximum drug concentration [59]. A similar protocol was used to prepare the INH-loaded MC and HA hybrid NPs (INH-MC/HA NPs). For the fluorescent-based confocal imaging, the blank NPs (CS/HA and MC/HA NPs) were loaded with rhodamine-B dye (Rh-B) to yield Rh-B CS/HA NPs and Rh-B MC/HA NPs.

4.2.7 Preparation of dry powders

4.2.7.1 Freeze-drying to obtain nanopowders

The nanosuspensions obtained in section 4.2.6 were freeze-dried to acquire dry nanopowders for inhalation. For freeze-drying, Scanvac, Coolsafe 100–9 pro-type apparatus (LaboGeneApS, Lyngø, Denmark) was used. The pressure was kept constant at 0.01. The parameters taken into account during freeze-drying are mentioned in table 6.

Table 6: Freeze-drying process parameters taken into consideration

Process	Time (h:min)	Chamber pressure (mbar)	Product temperature (°C)	Shelf temperature (°C)
Freezing	01:30	-----	-20	-40
	02:30		-20 to -26	
	03:45		-26 to -39	
Primary drying	04:00	0.01	-39 to -37	-25
	06:10		-37 to -31	-12
	09:40		-31 to -27	0
Secondary drying	16:00	0.01	-27 to -14	+9
	21:10		-14 to -6	+22
	40:15		-6 to -2	+30

4.2.7.2 Spray-drying to obtain nanopowders

The other drying technique used was spray drying. For this purpose, a Büchi nano spray dryer (B90 HP Büchi, Switzerland) was used. Mannitol and I400 were used as excipients in the spray drying because of their safety profile in the pulmonary drug delivery [60]. Mannitol and I400 improve the flow properties of the powders. In brief, CS was solubilized in 25 ml of 0.05 M glacial acetic acid. Also, HA solution was prepared together with INH in 50 ml of methanol: water (2:1). CS and HA polymeric suspensions were then mixed thoroughly. 4 % mannitol was added as an excipient to the suspension to obtain INH-CS/HA nanopowder with mannitol (CSM). A similar procedure was used for the MC-based formulation to acquire INH-MC/HA nanopowder with mannitol (MCM). The inlet temperature, outlet temperature, and peristaltic feed pump rate were set at 120 °C, 40 °C, and 20 % respectively [61]. The small-sized nozzle was utilized during the experiment. The polymeric suspension was driven through a peristaltic pump to the atomizer via compressed air pressure. The suspension was atomized by the nozzle which cycloned in the heated air to remove solvent and dry powder was deposited in the collection chamber which was scraped off and collected in an airtight container. Likewise, the nanopowders with I400 were developed by using similar protocol. For this case, 2 % w/v I400 was used as selected through thorough literature survey, to obtain INH-CS/HA nanopowder with I400 (CSI400) and INH-MC/HA nanopowder with I400 (MCI400). The preliminary procedure for the synthesis of the nanoparticles in case of freeze-drying and spray-drying was analogous and only the volume of the solvent and polymer concentrations were varied.

4.2.8 Drug loading (Percentage encapsulation efficiency)

To determine the % EE of the NPs, an indirect method was used. For this purpose, the nanosuspensions were centrifuged at 15,000 g for 20 min. The obtained supernatant was analyzed spectrophotometrically at 264 nm (λ_{max} for INH). The following equation 2, was then used to calculate the % EE,

$$\%EE = \frac{\text{Total drug-free drug}}{\text{Total drug}} \times 100 \quad [2]$$

4.2.9 Morphological, micrometric investigation and characteristics of powder

Scanning electron microscopy (SEM) (Hitachi S4700, Hitachi Scientific Ltd., Tokyo, Japan) was employed for the morphological investigation of the nanopowders obtained by the drying

methods at 2.0 at kV. The samples were mounted on the silica plates and gold-sputtered. During the whole experiment, the pressure was maintained at 1.3 to 13.0 mPa.

The particle size, PDI, and zeta potential of the nanopowders were investigated using Malvern zeta sizer Nano ZS (Malvern instrument, UK). The nanopowders were redispersed in the milli-Q water to obtain the nanosuspension. The samples were then analyzed at 25 °C using a quasi-elastic light scattering angle of 90°. Also, the bulk density and tapped density of the nanopowders were measured by a density tester (Stampf volumeter, STAV 2003, Germany). For this purpose, nanopowder was filled in the 5 ml tared graduated cylinder [62]. The method was adopted from the European Pharmacopeia, 2.9.3.4. Bulk density is the ratio of mass to volume (including inter particulate void), whereas tapped density is the density acquired by the mechanical tapping of the graduated cylinder. Also, Carr's compressibility index (CI) exhibiting the compressibility of powder, was calculated by using equation 3,

$$CI = \frac{\text{Tapped density} - \text{Bulk density}}{\text{Tapped density}} \times 100 \quad [3]$$

4.2.10 Physico-chemical investigations

4.2.10.1 Fourier transform infrared spectroscopy

Fourier transform infrared spectroscopy (FTIR) was performed to assess the compatibility of the polymers, cross-linker, drug, and bulking agents. FTIR (Thermo Nicolet AVATAR 330, USA) was employed to retrieve FTIR spectra. Briefly, samples were compressed into discs with KBr powder using a force of 10 kN with a hydraulic tablet press (Specac Ltd., UK). A 256-scan interferogram was obtained after the analysis of discs in the wavenumber range of 400 to 4000 cm^{-1} , at 4 cm^{-1} resolution.

4.2.10.2 X-ray powder diffractometry

X-ray Powder Diffraction (XRPD) measurements were recorded with Bruker D8 advance X-ray powder diffractometer (Bruker AXS GmbH, Germany) with Cu radiation at $\lambda=1.5406 \text{ \AA}$. VANTEC-1 detector was used to obtain the diffractograms ($3^\circ - 40^\circ 2\Theta$) at 40 mA. Samples were mounted on the glass substrate at 40 kV.

4.2.10.3 Differential Scanning Calorimetry

The thermal behaviour of the nanopowders was demonstrated by using Mettler Toledo DSC 821e (Mettler Inc., Schwerzenbach, Switzerland). The samples, approximately 3-5 mg, were hermetically sealed in the aluminium pans. An empty aluminium pan was used as a control.

The samples were heated in the range of 25 and 300 °C in an argon atmosphere at a heat flow rate of 5 °C/minute. STARE software (Mettler Toledo) was used to acquire the exotherms and endotherms.

4.2.11 *In vitro* studies

4.2.11.1 *Drug release study*

The release studies of the nanopowders were performed in the modified paddle method in the USP dissolution apparatus (SR8 plus dissociation test station, Hanson Research). All the studies were done in the simulated lung fluid (SLF) [63]. Briefly, 10 mg INH and nanopowders equivalent to 10 mg drug was dispersed in 100 ml SLF at 37 °C with 100 rpm rotation. After predetermined time intervals, 5 ml of the samples were withdrawn and centrifuged at 16,500 g for 10 min. The obtained supernatant was spectrophotometrically analyzed at 264 nm using a UV-visible spectrophotometer (Jasco V-730, Budapest, Hungary).

4.2.11.2 *Permeation study*

The permeation of the drug content was demonstrated by using a modified horizontal diffusion cell model (Grown Glass, New York). This in-house cell model comprised of the horizontally placed acceptor phase and donor chambers separated by an artificial membrane (Isopore™ membrane filter, 0.45 µm) impregnated with isopropyl myristate. Phosphate buffer (pH 7.4) was used in the donor chamber and SLF was used in the accepting chamber. Nanopowders equivalent to 10 mg of INH were dispersed in the donor chamber. The diffusion area was designed to be 0.69 cm² and the volume of media was kept constant in both the chambers [64]. The UV probe recorded the permeated drug in real-time, at 264 nm.

4.2.11.3 *Aerodynamic profile*

The aerodynamic profile of the nanopowders was evaluated by the Andersen cascade impactor (ACI) (Copley Scientific Ltd., Nottingham, UK). The aerodynamic profile corresponds to the mass median aerodynamic diameter (MMAD) and fine particle fraction (FPF). MMAD is the cut-off diameter of the particles deposited in the ACI whereas FPF < 5 µm corresponds to the particles theoretically deposited in the bronchial region and FPF < 3 µm corresponds to the particles deposited in the deeper lung and acinar tissues. ACI complies with the Ph. Eur. 2.9.18 (European Pharmacopoeia, 2015). The flow rate was kept constant (60 L/minute) by the vacuum pump (High-capacity pump model HCP5, Critical flow controller mode TPK, Copley Scientific Ltd., Nottingham, UK). Before the experiment, all the stages of the ACI, which

correspond to different cut-off diameters, were impregnated with a 1 % m/m solution of Span 80 and cyclohexane to simulate the humid environment of the lung [65]. Nanopowders equivalent to 10 mg of INH were filled into size 3 HPMC (hydroxy propyl methylcellulose) capsules and actuated through Breezhaler[®] dry powder inhalator device. The powder adhered to each stage of ACI was dissolved in ethanol: water (2:1) for the spectrophotometric analysis. MMAD and FPF were later measured.

Furthermore, the best sample was chosen based on the results and evaluated using the next-generation impactor (NGI). NGI is stated as the standard method for the evaluation of particle size distribution in the pulmonary passageways. Here, an optical method (microscope) was linked with NGI for the assessment of the settlement of NPs on each tray [66]. As mentioned earlier, nanopowder equivalent to 10 mg of INH was filled into HPMC capsules. A breath stimulator, a vacuum pump (HCP5 High-capacity pump; Copley Scientific Ltd., UK), an induction port mimicking the upper respiratory tract with a critical flow controller (TPK 2000; Copley Scientific Ltd., UK), and NGI (Copley Scientific Ltd., UK) are the main parts of the setup. Capsulated powdered drug sample was dosed from a Breezhaler[®] dry powder inhalator device. The impaction method was used to demonstrate the aerodynamic size distribution at different stages. The flow rate was maintained by TSI 4000 thermal mass flow meter. An in-house developed waveform generator was used as a breath simulator. For this purpose, a programmable logic controller (PLC) driven piston pump controlled the motor to generate airflows pattern (inhalation and exhalation).

4.2.12 *In silico* studies

The newest version of the Stochastic Lung Model (SLM) [67] was used to quantify the deposition of inhaled particles in terms of regional deposition fractions. For this purpose, the results obtained from ACI were employed in this *in silico* SLM. This numeric deposition model has been devised and validated for specific cases of aerosolized drugs [68]. The ratio of the mass of the particles deposited in the pulmonary passageways to the mass of particles in the capsule is termed as deposition fraction, which was numerically determined by SLM. This deposition fraction is classified into bronchial and acinar deposition fractions. The analytical method also determines the exhaled fraction, which is defined as the difference between the metered fraction (100 %) and a sum of the deposited fractions in the lungs and extra-thoracic pathways and the fraction lost in the inhalation device. This numeric integrated system tracks the particles till deposition and a large number of particles (usually 10^5) are tracked till

exhalation. The deposition profile is generated by the analytical formulas which take into account different considerations such as the straight passageways as well as the bent branches of the pulmonary system. The realistic measured geometric parameters and a Monte Carlo algorithm are used to simulate the inherent morphological stochasticity of the airways. Impaction, Brownian diffusion, or gravitational settling might be responsible for the deposition of particles. The characteristic of particles such as MMAD, FPF, and density along with inhalation parameters, i.e., the breathing rate of the patients are taken as inputs for this mode. For this Ph.D. work, two breath-hold times (BH) (5s and 10 s) were considered because the percentage of the inhaled powder depends on the inhalation pattern of the patient. The flow rate of 60 L/min was employed in an *in silico* modeling.

4.2.13 Colloidal stability in culture media

The colloidal stability of the nanopowders was studied in the cell culture media, RPMI with 10% (v/v) fetal bovine serum (FBS) supplemented with 1 % (v/v) penicillin-streptomycin-glutamine (PSG) and DMEM with 10% (v/v) FBS supplemented with PSG for 24 h at 4 °C. For this purpose, all the nanosuspension samples (1 ml) were dispersed separately in 5ml RPMI and DMEM media. Moreover, the stability of Rh-B labeled formulations were also studied in both the media. Size and PDI were recorded after the incubation time of 24 h, via zeta sizer.

4.2.14 Cell cultures

The cell lines used in the experiments, A549 and Raw 264.7 macrophages, were cultured in the DMEM supplemented with 10 % (v/v) FBS and 1 % (v/v) PSG. These cultures were incubated in a 5% CO₂ humidifier chamber at 37 °C. Moreover, the culture media was replenished after 3 days to maintain the cell confluency.

4.2.15 Macrophage isolation from human blood

The buffy coats were obtained from the Organ and Blood Donation Agency (ADOS; Santiago de Compostela, Spain). All the institutional and national guidelines for obtaining and using blood were followed. Blood was drawn from all the subjects after informed written consent. Permission was acquired from the Institutional Ethics Committee (Comité Ético de Investigación Clínica de Galicia, CEIC). Peripheral blood mononuclear cells (PBMC) were isolated by using the Ficoll density gradient separation method [69]. For this purpose, blood was transferred into a 50 ml tube under the laminar flow cabinet class II at room temperature and was diluted with PBS in a ratio of 1:1. Later, this blood was poured over Ficoll-Paque™

PLUS in a 2:1 ratio. This mixture was centrifuged at 400 g for 30 min at room temperature on deceleration mode by using Allerga X-12R, Beckman Coulter, to isolate the PBMC. With utmost care, the upper layer was discarded and the PBMC layer was transferred to a 50 ml falcon tube. This PBMC layer was centrifuged at 300 g for 10 min with PBS for washing. The washing ensures the purity of the cells by removing excess Ficoll media. PBMC cells were resuspended in RPMI-1640 supplemented with 2 % heat-inactivated FBS and 1 % PSG (R₂ medium). Following, the cells were then seeded at a density of 1.2×10^6 cells/ml into a 75 cm² cell culture flask for 2 h at 37 °C (5 % CO₂). The non-adherent cells were washed off after this incubation period using PBS and the adhered monocytes were cultured for 3 days in RPMI-1640 supplemented with 10 % heat-inactivated FBS and 1 % PSG (R₁₀ medium). This media was then replenished with R₁₀ medium along with 100 ng/ml cytokine; granulocyte-macrophage colony-stimulating factor (GM-CSF) after 3 days to differentiate the monocytes into macrophages.

4.2.16 *Ex vivo* studies

4.2.16.1 *Cytotoxicity studies*

For evaluation of cytocompatibility of the samples, an MTT assay was performed on the A549 cell line and Raw 264.7 cell line. A549 cells are the adenocarcinoma human alveolar basal epithelial cells and serve as a model for the pulmonary alveolar epithelia due to the dominance of alveolar type II cells. The recent progress in the TB studies has indicated that the alveolar epithelial cells also act as a niche for the M.Tb along with alveolar macrophages [70]. Hence, it was essential to assess the cytotoxicity profile of nanopowders on A549 cells. In the 96-well cell culture microplates, A549 cells were seeded at a density of 4×10^4 cells/well. CS/HA and MC/HA-based nanopowders were added to the wells at different concentrations followed by an incubation period of 24 h at 37 °C. MTT reagent (10 µl) was added to each well plate and incubated for 4 h. The formazan crystals formed were dissolved by adding 100 µl of isopropanol (100 µl of 0.04 N HCl in isopropanol). The OD was detected by EZ READ 400 ELISA reader (Biochrom, Cambridge, UK) at 550 nm. A similar protocol was adopted for the MTT assay on the Raw 264.7 macrophage cell line. For this purpose, the cells were seeded at a density of 1×10^4 cells/well. After seeding, the cells were incubated with different concentrations of nanopowders for 24 h. 10 µl of MTT was added to each well followed by incubation of 4 h. Later, 100 µl of acid propanol was added, and OD was measured at 570 nm using a microplate

reader (Synergy H1 Hybrid Multi-Mode, BioTek, Winooski, VT). 10% sodium dodecyl sulfate (SDS) was used as a positive control whereas the untreated 100% viable cells served as a negative control.

An MTS assay was performed to detect the cytotoxic behaviour of the samples [71]. For this purpose, the human blood-derived monocytes were differentiated into primary macrophages. These primary cells were then seeded on a 96-well microplate at a density of 1.10×10^5 cells/ml. After incubation of 24 h, the culture media was replaced with the different concentrations of the nanopowders and incubated for a further 24 h. SDS was used as a positive control and macrophages in culture media were used as a negative control with no toxicity. OD was measured at 490 nm using a microplate reader (Synergy H1 Hybrid Multi-Mode, BioTek, Winooski, VT). Equation 4 was used to calculate the % viability of the cells,

$$\text{Cell viability (\%)} = \frac{\text{Absorbance of sample}}{\text{Absorbance of control}} \times 100 \quad [4]$$

4.2.16.2 Blood compatibility study

The blood compatibility profile of the nanopowders was demonstrated by a hemolysis assay [72]. For this purpose, fresh blood from human donors was used. After washing the blood samples with PBS by centrifugation at 250 g for 5 min, the red blood cells (RBCs) pellet was obtained. The pellet was redispersed with PBS and the resulting suspension of cells was seeded on the 96-well plate. After an incubation period of 4 h and 24 h at 37 °C, the absorbance of the samples was read at 570 nm by using a microplate reader (Synergy H1 Hybrid Multi-Mode, BioTek, Winooski, VT). PBS served as a negative control whereas 1% v/v Triton-X served as positive control). Equation 5 was employed to calculate the % hemolysis of the samples,

$$\% \text{ hemolysis} = \frac{\text{Absorbance of sample} - \text{Absorbance of negative control}}{\text{Absorbance of positive control} - \text{Absorbance of negative control}} \times 100 \quad [5]$$

4.2.16.3 Cellular uptake of nanopowders (Qualitative and quantitative)

The visual intracellular uptake of nanopowders was demonstrated through a confocal laser scanning microscope (CLSM). The qualitative cellular uptake of nanopowders was studied in A549 cells and Raw 264.7 macrophages. For this study, the cells were seeded onto the individual Lab-Tek® chambered #1.0 borosilicate cover glass system and incubated for 24 h. Later, the culture media was replaced with 300 µl of (10 µg/ml of nanopowder concentration) Rh-B labeled nanosuspension and incubated for 2 h. 4% paraformaldehyde (15 min incubation) was added to each glass chamber following the washing of the cells with PBS. Formaldehyde

was added for the fixation of cells. Washing of the cells with PBS was repeated and DAPI dye (300 μ M, 1:500 in PBS) was added for staining nuclei with an incubation of 50 min. Excess DAPI dye was washed off with PBS and mounting media was added to each glass chamber to perform imaging by CLSM (Leica SP5, Mannheim, Germany). Untreated cells were kept as a control. A similar protocol was adopted for quantitative uptake followed by analysis through flowcytometry in a BD FACSCalibur cytometer. Rh-B 546/568 (Ex/Em), DAPI 359/457 (Ex/Em).

4.2.16.4 Macrophage phenotype analysis

The primary human macrophages were cultured and incubated with nanopowders (10 μ g/ml). After an incubation period of 24 h, the cells were washed with PBS to remove the NPs. These cells were then resuspended in PBS and stained with antibodies (CD80-PE and CD83-APC) with incubation for 25 min at -4 °C in dark. After incubation, the cells were washed and resuspended in PBS and kept on ice till the quantification study. The maturation markers' level was quantified by flowcytometry in a BD FACSCalibur cytometer. For analysis of data, flowing software (Cell imaging core, Turku Centre for Biotechnology) was used.

4.2.16.5 Tolerogenic activity of NPs

2,3-Indoleamine dioxygenase (IDO) is an immunosuppressant enzyme responsible for the catabolism of tryptophan and essential to the growth of microorganisms that affects the T-cell tolerance. Also, IDO is responsible for the apoptosis of Th1 cells by catabolizing tryptophan into kynurenine [73]. IDO assay is hence a quantification assay for the detection of kynurenine in the culture media. The protocol was adapted from the literature to demonstrate the tolerogenic activity of NPs [74]. For this purpose, 1×10^4 primary macrophages were seeded and incubated on the 48-well plate with different formulations (final volume 0.5 ml). 1.25 μ l of 100 μ M L-tryptophan was added to the plates at least 4 h before the end of the incubation period. Culture media was obtained after centrifugation of cells at 10,000 g for 5 min at room temperature and 30% trifluoroacetic acid was mixed with this obtained culture media to facilitate the precipitation of cell debris. Centrifugation was repeated with the aforementioned parameters and obtained supernatant was mixed with Ehrlich reagent (1% v/v) and absorbance of the samples was analyzed through a microplate reader at 490 nm.

5. RESULTS AND DISCUSSION

5.1 Synthesis, quantification, and characterization of polymer

The number of mannose groups on the polymer was found to be $212 \pm 27 \mu\text{M}$ per gram of MC. Moreover, the thiol groups anchored to the MC were quantified to be $328 \pm 11 \mu\text{M}$ per gram, and disulfide bonds were quantified to be $74 \pm 21 \mu\text{M}$ per gram of MC. NMR spectra (Figure 2) revealed the conjugation of mannose to CS with a peak at 4.03 ppm corresponding to the methylene protons of the mannose sugar [75]. The acetamido group between mannose and chitosan by Schiff's base reductive amination is represented by the peak at 2.404 ppm (corresponding to the protons of CH_2 - group of linkage) [76]. The amine group of CS was indicated at 0.859 ppm and the peak at 1.631 ppm corresponded to the methyl group of the non-deacetylated CS [77].

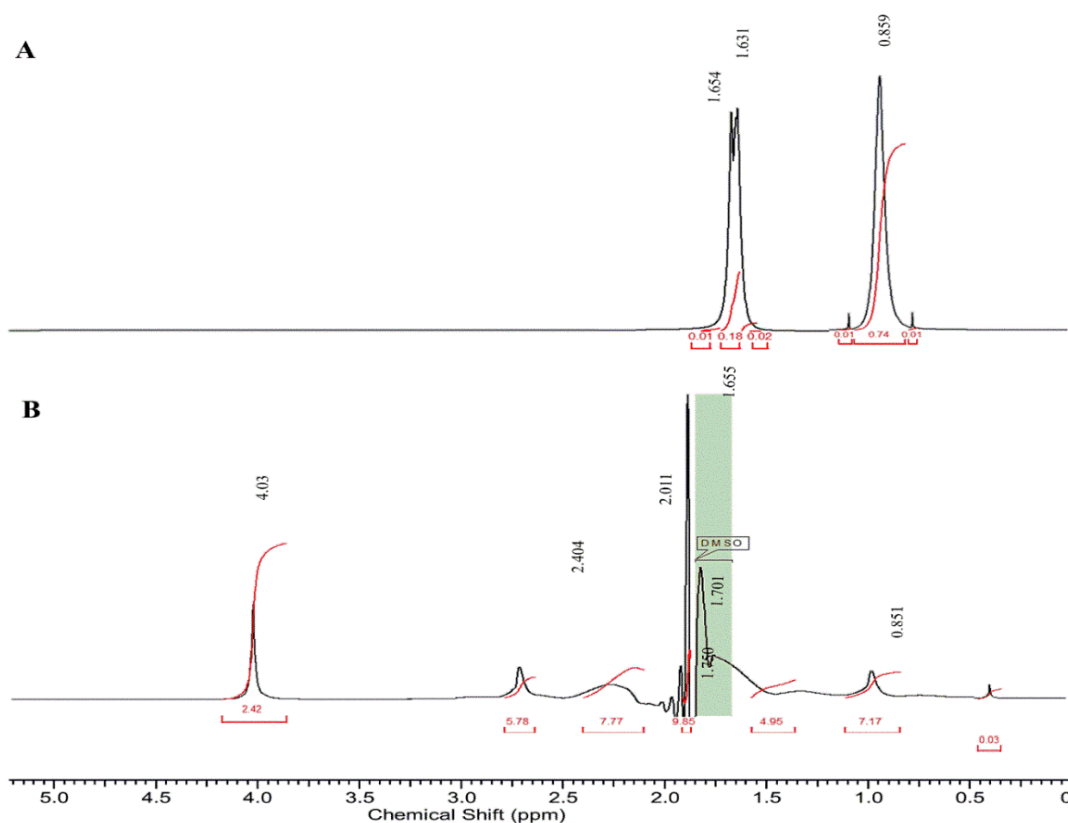


Figure 2: NMR spectra of (A) chitosan and (B) mannosylated chitosan

5.2 QbD and knowledge space of nanosuspensions

QbD provided a robust approach to scrutinize the critical factors that were found to influence the QTPP. Figure 3 mentions the scrutinized parameters such as CMAs, APPs, CQAs, and QTPPs along with their interdependence association. Later, Lean QbD software[®] was employed

to perform the interdependency between the critical attributes, as shown in the figure. Based on this relation, the critical CQAs affecting the QTPPs were chosen. Similarly, the CQAs critically influencing CMAs and CPPs were also selected.

QTPPs \ CQAs	Therapeutic indication	Target population	Route of administration	Site of activity	Dosage form	Dissolution Profile
PDI	High	Low	High	High	High	Low
Size of API	High	Low	High	High	High	Medium
Appearance	High	Low	High	Low	High	High
Dissolution	High	Low	Medium	Low	Medium	High
Toxicity/Irritation	High	High	High	High	High	Low
Solubility	Low	Low	Medium	Low	Medium	High
Zeta potential	High	Low	Low	High	Low	Low
Permeability	High	Low	High	High	High	Low
Stability	Low	High	Medium	Low	High	Low
Encapsulation efficiency	High	Low	High	High	High	High

CPPs and CMAs* \ CQAs	Sonication speed	Sonication time	pH	Excipients	Ratio of polymer	API characteristic
PDI	High	High	High	High	High	Medium
Size of API	High	High	High	High	High	Medium
Appearance	Low	Low	High	Medium	Medium	Low
Dissolution	High	High	High	High	High	High
Toxicity/Irritation	Low	Low	Low	High	High	High
Solubility	Low	Low	High	Medium	Medium	High
Zeta potential	Low	Low	High	High	High	High
Permeability	Medium	Medium	High	High	High	High
Stability	Low	Low	High	High	High	High
Encapsulation efficiency	High	High	High	High	High	High

Figure 3: The selected QTPPs, CMAs, CPPs, and CQAs and the interdependence of these critical factors as part of risk assessment.

5.3 DoE for optimization of nanosuspensions

The critical chosen parameters are listed in table 7. The highly influential CMAs and CPPs were prioritized by using DoE using BB factorial design. Different formulations were prepared according to the number of experimental runs recorded by STATISTICA® 10 software and these runs were studied against the dependent outcomes such as size, PDI, and zeta potential. This robust method was used for developing the nanosystem using CS polymer and was repeated with the same parameters for the MC-based systems due to the same origin of the polymer. Later, similar parameters were taken into consideration for freeze-drying and spray-drying to develop nanopowders. The results of the dependent variables against the different runs are mentioned in table 8.

Table 7: Level of selected critical factors

Critical Factors	Levels		
	Low	Medium	High
X ₁ : HA concentration (mg)	2.5	5.0	6.5
X ₂ : CS concentration (mg)	1.25	2.5	3.25
X ₃ : Pulse ratio	30	40	50

Subsequently, DoE gave Pareto charts as an outcome which highlighted the relative importance of the individual and relative effects in the liner (L) and quadratic (Q) models. Pareto charts (figure 4) demonstrate the probability of the influence of critical variables on the dependent variables individually. A T-test was used during this study to determine the level of significance. The vertical line shows the significant variables with a correlation to dependent variables.

Table 8: The results of dependent variables obtained through 15 runs by Box-Behnken design in STATISTICA® 10 for CS/HA NPs

Run codes	HA (mg)	CS (mg)	Sonication pulse ratio	Average size (nm)	PDI	Zeta potential (mV)
C1	6.5	2.5	30	390	0.417	30.5
C2	5.0	3.25	30	399	0.432	28.2
C3	2.5	1.25	40	324	0.202	27.8
C4	5.0	1.25	30	387	0.391	30.6
C5	5.0	2.5	40	342	0.199	34.3
C6	5.0	2.5	40	346	0.187	32.1
C7	6.5	3.25	40	457	0.451	28.5
C8	5.0	1.25	50	363	0.215	29.8
C9	2.5	3.25	40	398	0.331	28.5
C10	6.5	1.25	40	375	0.411	31
C11	2.5	2.5	30	330	0.216	19.5
C12	5.0	3.25	50	390	0.185	27.9
C13	5.0	2.5	40	351	0.214	28
C14	2.5	2.5	50	308	0.204	22.2
C15	6.5	2.5	50	415	0.398	27.5

Furthermore, the surface plots (figure 5) were acquired from the STATISTICA software. The 3D plots show that the size and PDI of the formulations increase with an increase in the concentration of the polymers. The optimal concentrations of the CS and HA polymers were determined to be 5 mg and 2.5 mg respectively. On the other hand, the zeta potential values

altered significantly by varying the concentration of HA. The established second-degree polynomial model for the estimation of Y_1 (size), Y_2 (PDI), and Y_3 (zeta potential) for the nanoformulations was determined as given below

$$Y_1 = 373.1 + 69.2X_1 + 48.72X_2 - 11.3X_3 + 0.235X_1X_2 + 20.912X_1X_3 + 10.088X_2X_3 - 17.74X_1^2 - 39.18X_2^2 - 5.34X_3^2 \quad [6]$$

$$Y_2 = 0.311 + 0.187X_1X_1 + 0.05X_2 - 0.11X_3 - 0.05X_1X_2 - 0.03X_1X_3 - 0.01X_2X_3 - 0.09X_1^2 - 0.08X_2^2 - 0.03X_3^2 \quad [7]$$

$$Y_3 = 27.5 + 4.98X_1 - 1.414X_2 - 0.025X_3 - 0.088X_1X_2 - 2.80X_1X_3 + 0.20X_2X_3 + 2.75X_1^2 - 0.65X_2^2 + 3.19X_3^2 \quad [8]$$

The particle size (Y_1) was most predominantly affected by the concentration of CS and HA with sonication speed not affecting the average diameter of particles. The PDI (Y_2) was significantly influenced by the concentration of CS and HA. As the concentration of the polymers increased, there was a significant increase in the PDI leading to aggregated sample. Zeta potential (Y_3) was most directly influenced by the increase in the concentration of HA.

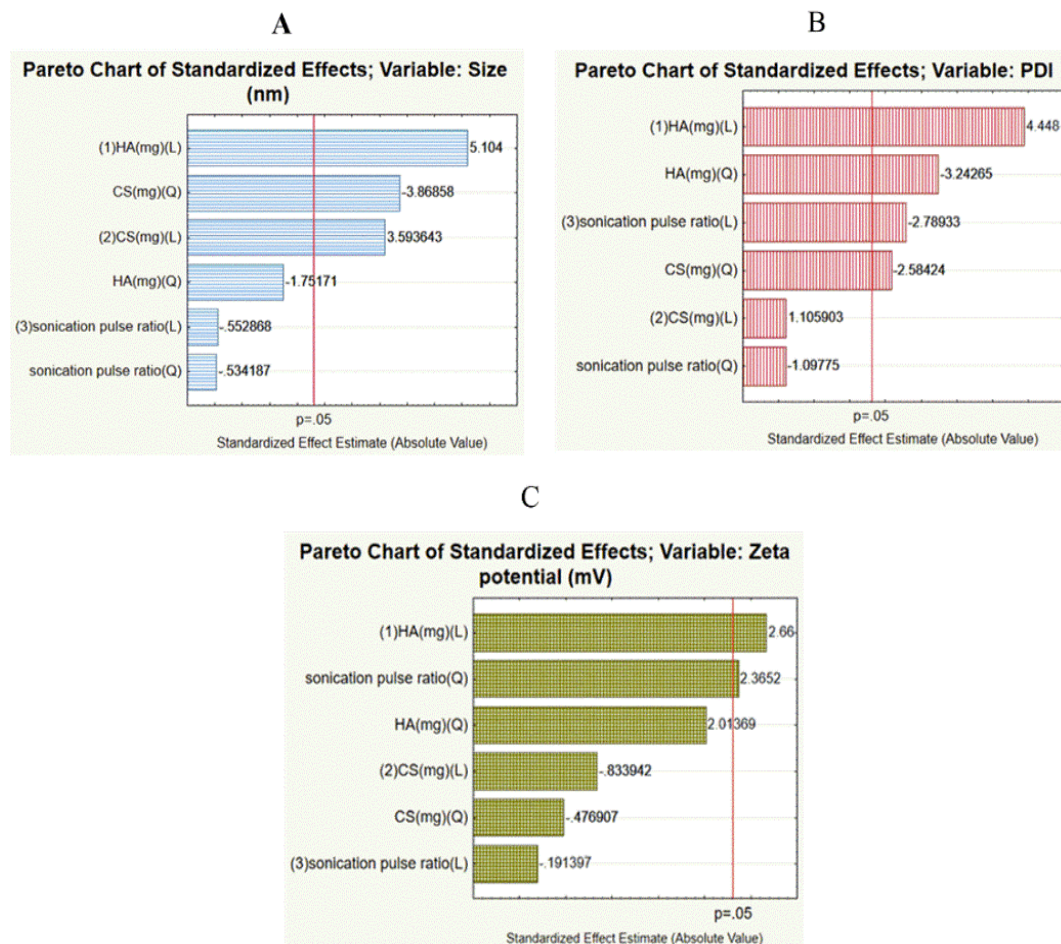


Figure 4: The independent variables (concentration of CS, HA, and sonication speed) and their desired outcomes in the form of (A) size, (B) PDI, and (C) zeta potential, as Pareto charts. Bars exceeding the vertical line show that the terms are significant ($p < 0.05$).

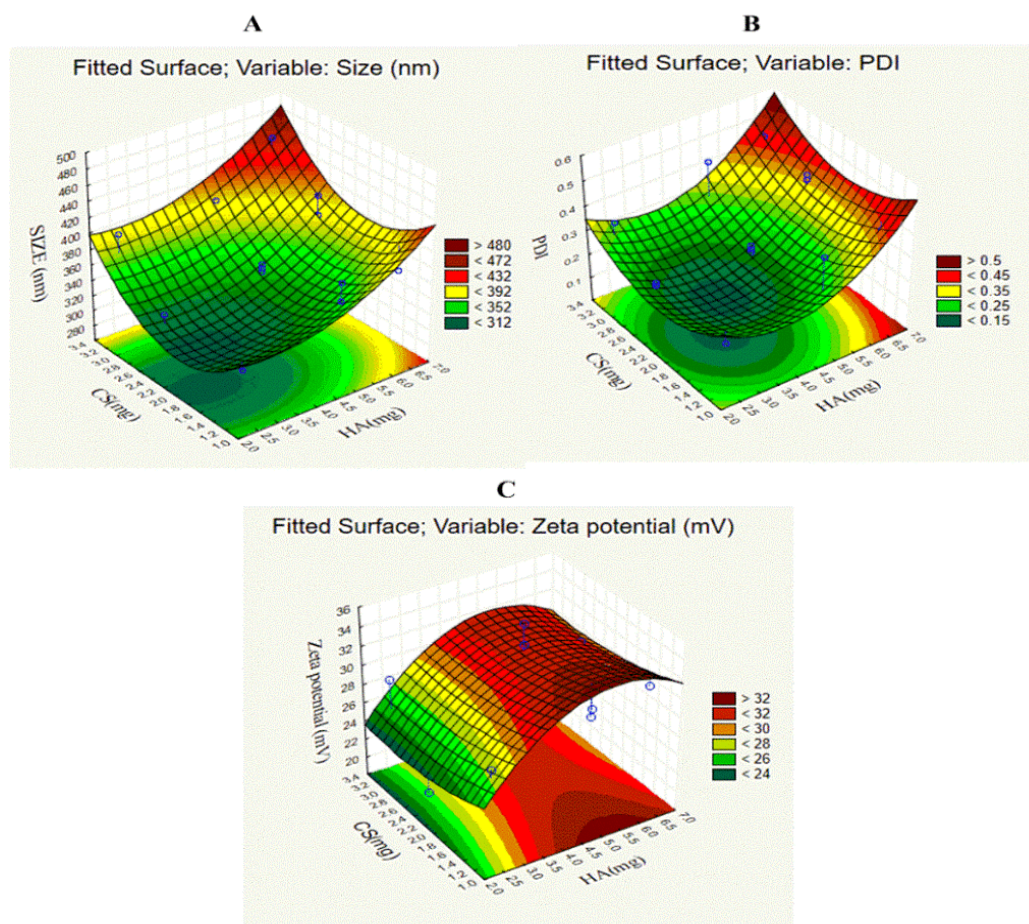


Figure 5: 3D surface response plots demonstrating the influence of CS, HA, and sonication speed on the (A) size, (B) PDI, and (C) zeta potential of the nanoformulations.

Following, the samples prepared were freeze-dried and spray-dried to obtain the nanopowders and again the particle size, PDI, and zeta potential were determined. For this purpose, the nanopowders were redispersed in the milli-Q water and were analyzed using a zeta sizer. The outcomes are reported in Table 9.

5.4 Drug loading (Percentage encapsulation efficiency)

The encapsulation efficiency for the freeze-dried and spray-dried samples was quantified. The freeze-dried nanopowders exhibited a high % EE. It was assumed that the subsequent loading of INH after the synthesis of NPs was an effective strategy, as the drug was loaded into the voids of the plexus formed on the surface of NPs as a result of ionic gelation. However, the synthesis of NPs simultaneously with drug loading yielded lower % EE, in the case of spray-drying. The % EE for all the samples has been mentioned in table 9.

Table 9: The size, PDI, zeta potential, and % EE of the optimized nanopowders

Parameters	MCM	MCI400	MC/HA	CSM	CSI400	CS/HA
Average size (nm)	316 ± 25	323 ± 15	302 ± 11	404 ± 10	299 ± 19	300.2 ± 11
Zeta potential (mV)	21.4 ± 4.01	14.5 ± 0.93	31.2 ± 2.35	18.4 ± 6.01	24.1 ± 5.50	30.1 ± 3.13
PDI	0.215 ± 0.91	0.398 ± 1.5	0.211 ± 2.89	0.246 ± 0.07	0.310 ± 1.01	0.204 ± 0.01
Encapsulation efficiency (%)	74.05 ± 8.22	63.45 ± 2.84	90.17 ± 1.01	72.43 ± 2.41	59.66 ± 1.84	91.21 ± 2.31

5.5 Morphological investigation and characteristics of powder

As shown in figure 6, the freeze-dried nanopowders did not present smooth-surfaced morphology. Also, the freeze-dried samples had patches of aggregation. On the other hand, the spray-dried samples with mannitol demonstrated smooth mono-dispersed particles. However, using I400 yielded particles with aggregated appearance.

The powder flow characteristics are mentioned in table 10. The bulk densities and tapped densities measurements were found to be good for the aerosolization of samples. The CI values < 25 % highlight good powder flow properties. On the contrary, an increase in the CI is the result of the cohesive forces between the nanopowders. CI values for the freeze-dried nanopowders were found to be high for the CS/HA NPs but the CI for MC/HA NPs was within an acceptable limit. The only sample which was found to be promising in terms of rheological characteristics was MCM, which was later chosen for the high-end aerodynamic *in-vitro* test using NGI.

Table 10: Powder flow characteristics of the freeze-dried and spray-dried nanopowders

Parameters	MCM	MCI400	MC/HA	CSM	CSI400	CS/HA
Bulk density (g/cm ³)	0.208 ± 0.88	0.134 ± 0.13	0.081 ± 1.47	0.089 ± 0.05	0.116 ± 0.43	0.118 ± 2.01
Tapped density (g/cm ³)	0.260 ± 0.01	0.181 ± 0.07	0.108 ± 0.19	0.130 ± 1.33	0.150 ± 0.09	0.203 ± 0.77
Carr's index (%)	20 ± 0.51	25.71 ± 1.21	25 ± 0.13	31.8 ± 0.05	22.45 ± 0.09	42 ± 0.99

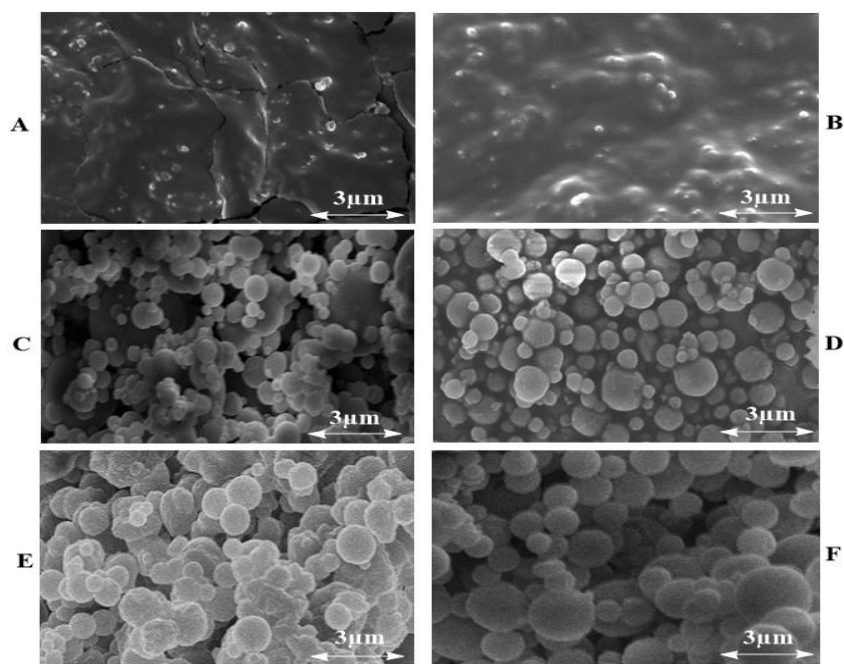


Figure 6: Scanning electron microscopy (SEM) micrographs of the freeze-dried and spray-dried nanopowders. (A) CS/HA NPs, (B) MC/HA NPs, (C) CSI400, (D) CSM, (E) MCI400 and (F) MCM.

5.6 Outcomes of physicochemical investigation

5.6.1 Fourier transform infrared spectroscopy

FTIR experiment demonstrated the compatibility between the components of the freeze-dried and spray-dried nanopowders. Firstly, the mannose conjugation to CS (Figure 7A) was confirmed by the mannose band stretch at 850 cm^{-1} , an amide bond stretching at 1100 cm^{-1} and COO symmetric stretch at 1200 cm^{-1} [78]. All the freeze-dried and spray-dried samples composed of MC exhibited the corresponding peaks of MC. Similarly, all the nanopowders comprised of CS highlighted the peaks of CS such as CO-NH₂ fingerprint peak at 1600 cm^{-1} and OH bond widening at 3500 cm^{-1} . Likewise, the IR peaks for HA can also be observed in all the samples which were pictured at 1400 cm^{-1} as carbohydrate symmetric stretch. The loaded drug INH displayed the characteristic peaks at $3000\text{--}3300\text{ cm}^{-1}$ corresponding to NH₂-NH₂ band stretch and at 1700 cm^{-1} related to C=N and C=O.

For the freeze-dried samples, the peak of cross-linker TPP was shown at 1156 cm^{-1} characteristic of asymmetric and symmetric stretch of PO₂ group (Figure 7A). For the spray-dried samples with mannitol, the characteristic peaks were exhibited at 1400 cm^{-1} and 3300 cm^{-1} [79]. The characteristic IR peaks for I400 were demonstrated at 1400 cm^{-1} and 1200 cm^{-1} in spray-dried nanopowders with I400 [80] (Figure 7B). Altogether, the components of the

nanopowders were found to be stable and physicochemical compatible during the development of nanopowders.

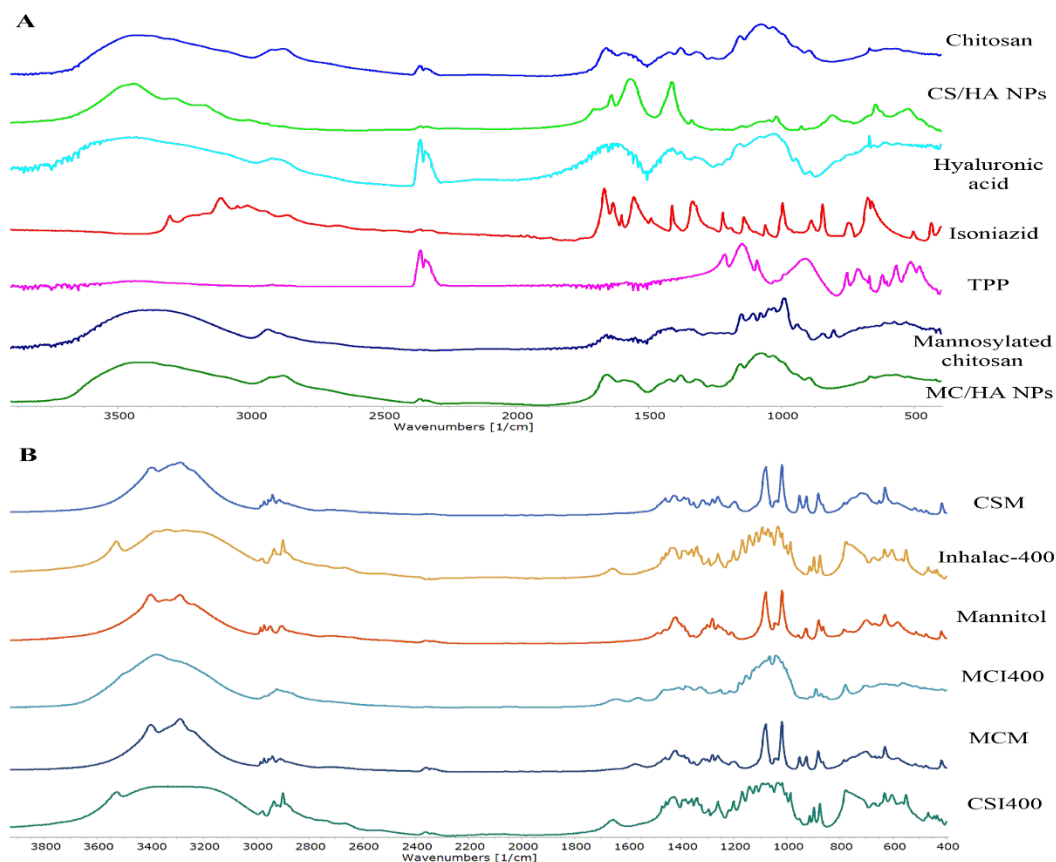


Figure 7: IR spectra of (A) freeze-dried and (B) spray-dried nanopowders

5.6.2 X-ray powder diffractometry

XRPD analysis (Figure 8) was conducted to understand the physical nature of the components before and after the synthesis of nanopowders. The XRPD images of freeze-dried samples did not exhibit any discrete crystalline peaks that were initially present in the nascent INH between 10° and 40° . Similarly, the crystalline peaks for INH were not found in the spray-dried nanopowders as well which can be related to the fact that INH changed to an amorphous state upon encapsulation. The spray-dried nanopowders displayed the 2θ peak from 10° to 20° , indicating that mannitol existed as a crystalline excipient before and after the drying process [81]. I400 spray-dried nanopowders revealed a similar behaviour by showing the discrete peaks of I400 between 16° and 22° and therefore, it can be mentioned that spray-drying did not alter the crystallization behaviour of the excipient [82]. The behaviour was further investigated by the thermal analysis.

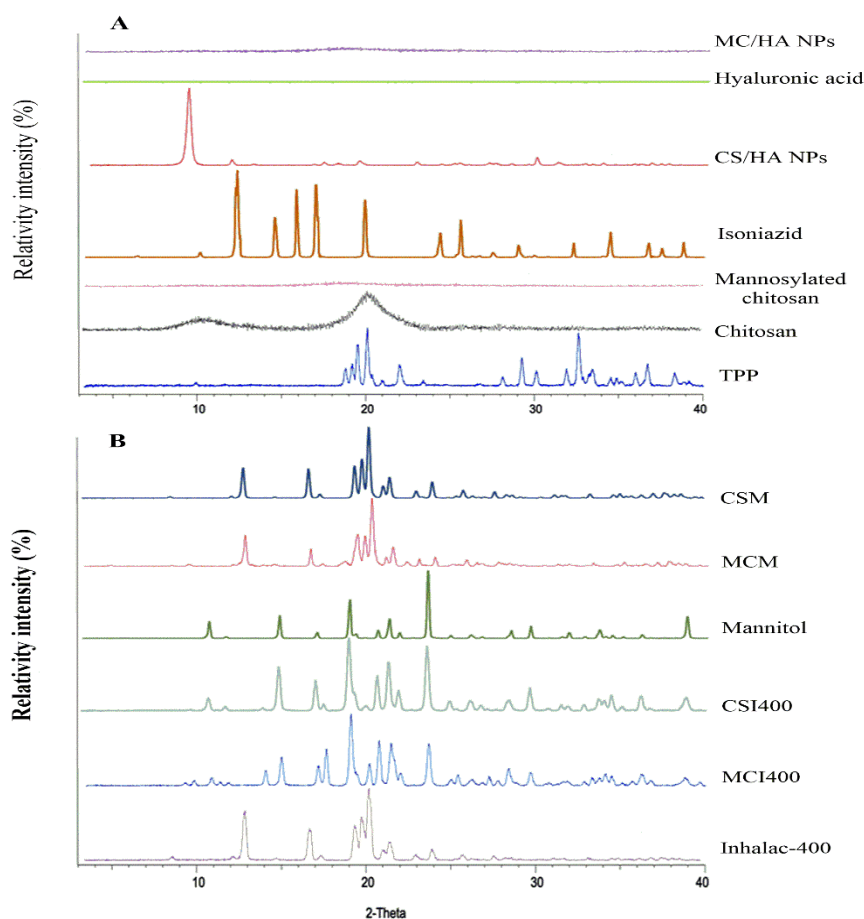


Figure 8: XRPD diffractogram of (A) freeze-dried and (B) spray-dried nanopowders

5.6.3 Differential Scanning Calorimetry

The Differential Scanning Calorimetry (DSC) curves (Figure 9) identify the thermal behavior of the components of the nanopowders. The DSC curve of INH exhibited an endothermic peak at 171.07 °C highlighting the melting point [83]. However, this endotherm was not present in the freeze-dried and spray-dried samples revealing the intact physical stability of the drug inside the NPs. Mannitol exhibited an endothermic peak at 169 °C corresponding to the melting point. This endothermic peak was present in the spray-dried samples with mannitol showing the melting of the mannitol during the drying process [62], followed by recrystallization which was confirmed by the XRPD sharp diffractogram. On the contrary, no such sharp change was observed for the I400 spray-dried samples. But two small endothermic peaks at 145 °C and 213 °C were seen which demonstrated the loss of bound water [84]. These peaks were also seen in the nascent I400. The results were by the literature and did not exhibit any sharp morphological or chemical changes during the process of drying.

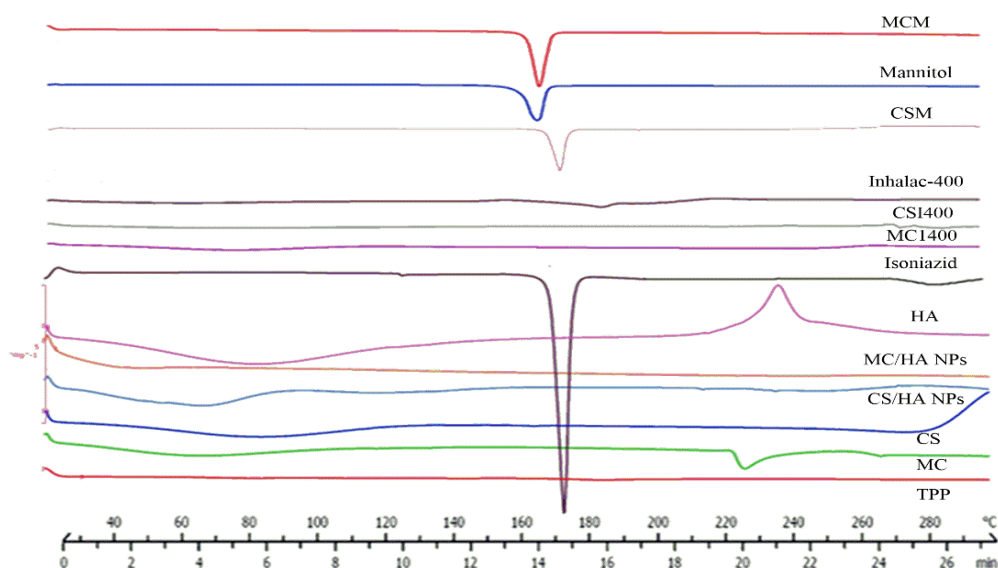


Figure 9: DSC curves for the freeze-dried and spray-dried nanopowders, Exo ↑

5.7 Results of *In vitro* studies

5.7.1 Drug release study

All the release studies were performed for a period of 48 h under similar conditions, i.e., at body temperature. The unmodified INH was released in the media completely in 5 h. On the other hand, the release was modified in the nanopowders. It can be observed from Figure 10, that the release of INH was slowed down as the polymeric composition changed from CS to MC, 63% to 40 %, demonstrating that mannosylation facilitates the controlled release [85]. However, there was no significant change in the release patterns of INH from the spray-dried and freeze-dried samples. Overall, the controlled release of the drug is favourable for chronic infections which otherwise need frequent drug administration to maintain the adequate drug concentration at the target site.

5.7.2 Permeation study

The diffusion cell model employed to study the concentration of permeated drug in the acceptor media ensures the homogenous distribution of the sample in the donor phase at a constant temperature. The nano-dimensional surface of particles possesses a large surface area available for the release of drug followed by permeation via effective passive diffusion. Approximately 58-72 $\mu\text{g}/\text{cm}^2$ of INH was able to permeate across the membrane filter into the acceptor phase in 2 h, for the MC-based samples irrespective of the drying technique (Figure 11).

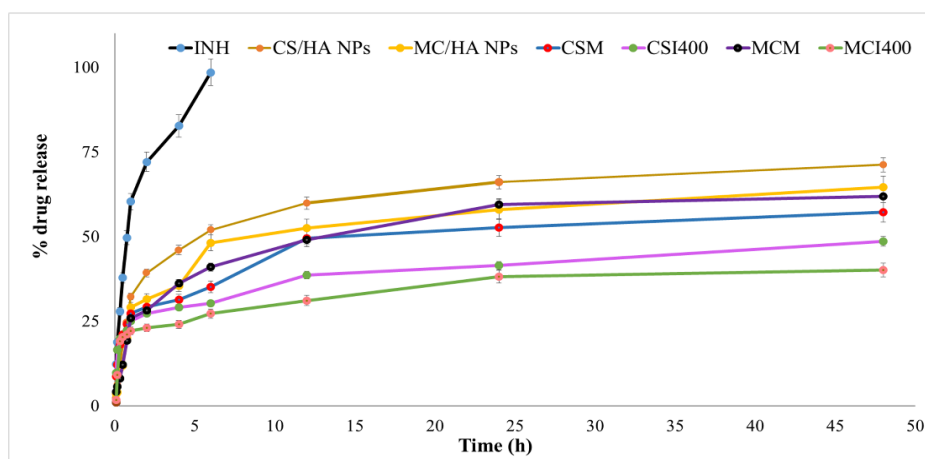


Figure 10: The *in vitro* release of INH from freeze-dried and spray-dried nanopowders, in the simulated lung media (pH 7.4)

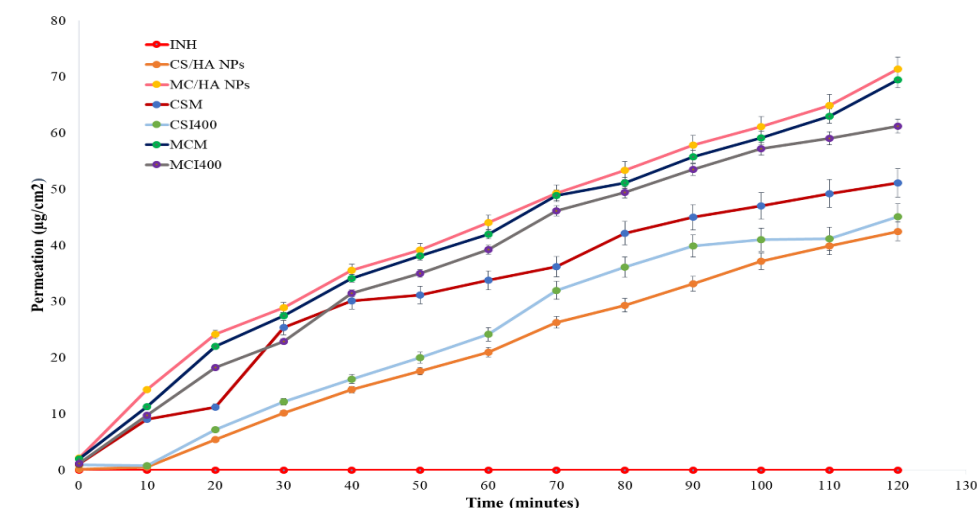


Figure 11: The *in vitro* permeation profile of INH ($\mu\text{g}/\text{cm}^2$) from the freeze-dried and spray-dried nanopowders from donor to acceptor chamber

A slight visible difference was observed in the permeation pattern of INH from the CS-based nanopowders, with a maximum concentration of 46–48 $\mu\text{g}/\text{cm}^2$ for CSM. A similar trend was observed for the CSM highlighting that mannitol can somehow improve the permeation of the drug [86]. Also, mannosylation improves the permeation profile in isopropyl myristate (mimicking the pulmonary environment) impregnated membrane to ameliorate the absorption. [87].

5.7.3 Aerodynamic profile

The aerodynamic profile as investigated by ACI presented the favorable MMAD of the nanopowders (Table 11). MMAD values for freeze-dried nanopowders, CS/HA NPs, and

MC/HA NPs were found to be 2.67 μm and 2.981 μm respectively. Similarly, the MMAD for the spray-dried nanopowders ranged between 1.632 μm - 3.556 μm . FPF <5 μm was observed to be high (80 %) for the MCM nanopowder revealing that the use of mannitol along with polymer MC produced the fine particles. This meant that more than 80 % of the particles in the powder were less than 5 μm in dimension and had a tendency to deposit in the upper parts of the lungs (particles in the range of 1.1 - 4.7 μm are deposited in stage 2 - 5 of ACI). FPF < 3 μm was also found to be the highest (69 %) for the sample MCM.

The particles below the range of 3 μm have a higher tendency to deposit in the bronchial as well as the alveolar region. Later, the best sample (MCM) was chosen for the evaluation by NGI. MCM nanopowder was evaluated in terms of mass size distribution and the results were fetched based on the surface coverage of the collection plates. The data (Figure 12) presented that the average mass size distribution of more than 50 % of the particles had a size of 1.37 - 2.3 μm . The results demonstrated that a higher fraction of the particles were in a similar range as observed via ACI testing.

Table 11: The aerodynamic parameters of freeze-dried and spray-dried samples as determined by ACI

Parameters	MCM	MCI400	MC/HA	CSM	CSI400	CS/HA
MMAD (μm)	1.632 \pm 0.11	2.464 \pm 0.23	2.981 \pm 0.12	3.556 \pm 0.24	2.891 \pm 0.09	2.67 \pm 0.05
FPF <5 μm (%)	80.94 \pm 0.66	74.89 \pm 0.16	69.01 \pm 0.05	62.73 \pm 1.8	68.94 \pm 0.19	62.11 \pm 1.06
FPF <3 μm (%)	69.46 \pm 0.97	59.14 \pm 1.11	50.11 \pm 0.18	44.04 \pm 0.19	50.91 \pm 0.61	68.70 \pm 0.11

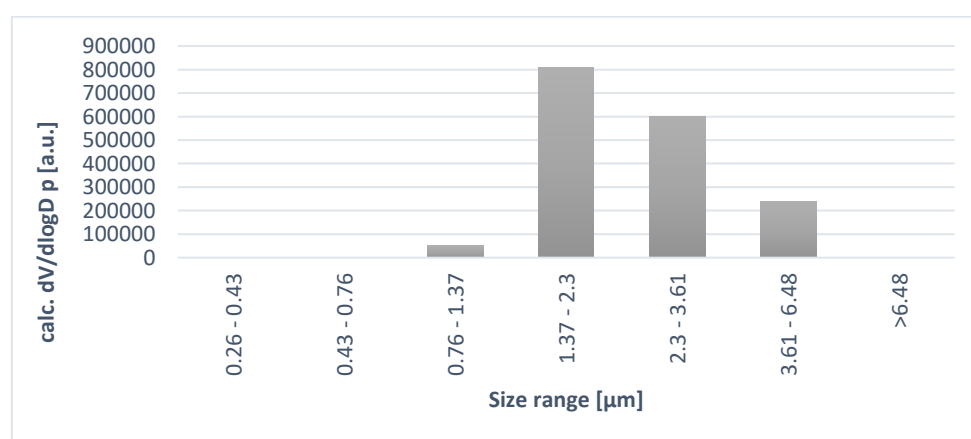


Figure 12: Mass size distribution of deposited particles in the NGI based on the surface coverage area of plates

5.8 Discussion of *in silico* studies

The *in silico* stochastic lung modeling was used to determine the exhaled fraction of the nanopowders (EXH), the extra-thoracic fraction of the drug (ET) referring to the deposition in the extra-thoracic airways and the fraction of nanopowders deposited in the bronchial and acinar regions termed as LUNG. As shown in figure 13, approximately, 30 % of the nanopowders were deposited in the extra-thoracic region for all the freeze-dried samples irrespective of BH time.

On the contrary, the results varied for the ET fraction of spray-dried samples in the range of 14-41 %. Similarly, EXH was presented to be higher in the case of spray-dried samples, especially for I400-based nanopowders. However, MCM demonstrated better aerodynamic characteristics in the model, by presenting low EXH with high ET and LUNG fraction than all the other spray-dried nanopowders, by increasing BH time. Moreover, mannitol was found to be a promising excipient for spray-drying for the pulmonary inhalation dosage forms as compared to I400, based on the results.

Surprisingly, freeze-drying yielded nanopowders which depicted a good deposition profile with a low EXH fraction. Besides, the LUNG and ET fraction was also found to be high for the freeze-dried samples, irrespective of the composition. Overall, the *in silico* deposition profile correlated well with the *in vitro* deposition study.

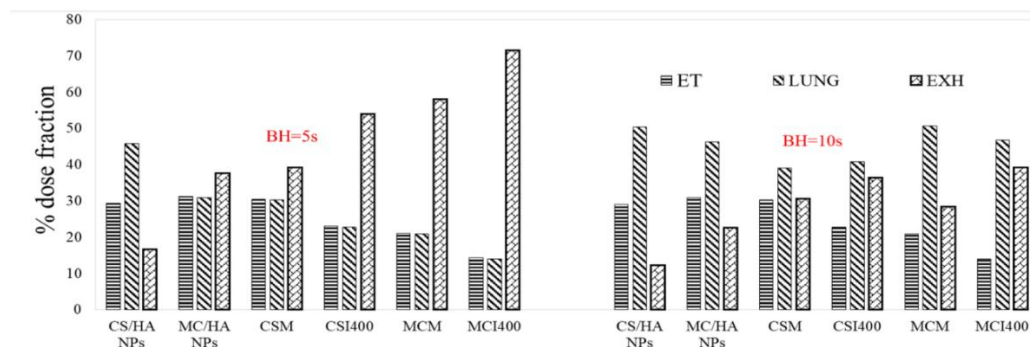


Figure 13: Presentation of *in silico* deposition modeling at two breath-hold (BH) times, for the freeze-dried and spray-dried nanopowders. [ET: fraction of the nanopowder deposited in the extra-thoracic airways, LUNG: cumulative fraction of nanopowders deposited in the bronchial and acinar region, EXH: exhaled fraction of the nanopowders].

5.9 Results of colloidal stability in culture media

To take account of the behavior of the nanosystem in the cell culture during the ex-vivo studies, the colloidal stability of the nanopowders was tested in RPMI and DMEM media. The results,

as shown in figure 14, show that there is a slight change in the PDI of the particles. The possible reason for this increase in the PDI on incubation for a long time can be due to the presence of salts in the media. The presence of ionic charge in the media was responsible for the cohesive forces and hence the low dispersity of the particles. The nanosuspensions exhibited a homo-dispersive nature as can be seen from the PDI index values < 0.7 [88]. Similar behavior was observed for the size measurements.

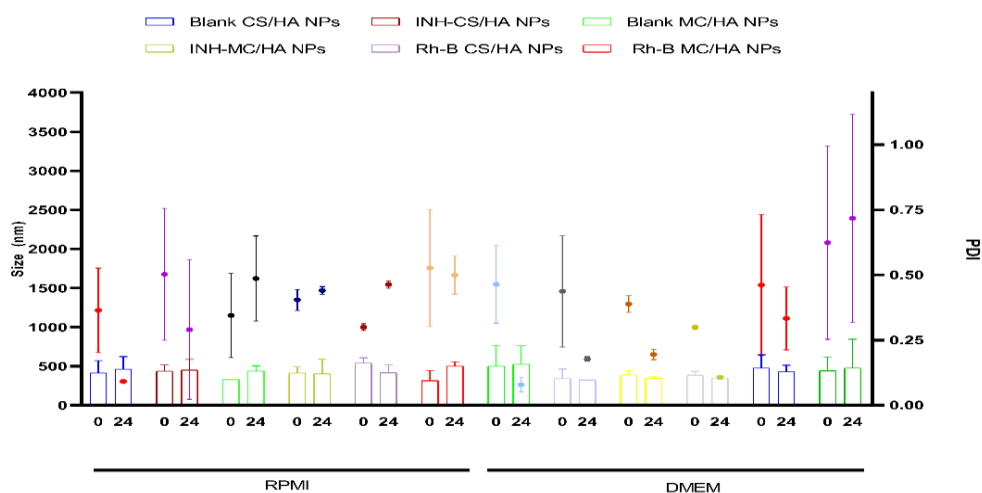


Figure 14: Stability of the nanosuspensions in RPMI and DMEM with the relative change in particle size (nm), zeta potential (mV), and polydispersity index (PDI) over 24 h. Bars=size; Dots= PDI (n=2)

There was found to be a relative increase in the size of the NPs that may also be contributed to the detection of electronic cloud (due to ions in culture media) around the particle in the zeta sizer. Altogether, results did not deviate remarkably and the formulations were considered to be stable, even though the measurements were performed with a lag time of 15 days due to the pandemic. Results are expressed as mean \pm SEM, $n=2$.

5.10 Evaluation of *ex vivo* studies

5.10.1 Cytotoxicity studies

The toxicity profile of the nanosuspensions on the different cells was evaluated by MTT assay. Different concentrations (0.01 mg/ml, 0.5 mg/ml and 1 mg/ml) of the nascent drug i.e., INH were used for the assay together with an equivalent concentration of the nanosuspensions corresponding to 0.01 mg/ml, 0.5 mg/ml and 1 mg/ml of INH. For the A549 cells, almost all the samples demonstrated the viability of more than 80 %, and MC-based nanosystems exhibited up to 100 % viability of cells (Figure 15A). On the contrary, the cytotoxicity of the

nanosuspensions on the Raw 264.7 macrophages was found to be concentration-dependent. The low concentrations of INH, i.e., 0.5 mg/ml and 0.01 mg/ml exhibited more than 50 % cell viability but it was cytotoxic to the Raw 264.7 macrophages at high concentrations (Figure 15B). The variation in the cytotoxicity may also be attributed to the change in the polymeric concentrations. Altogether, all the nanosuspensions had viability percentages above the threshold percentage of 50 %. Likewise, the cytotoxicity studies on the primary human macrophages derived from human blood highlighted similar behavior (Figure 15C). The results were evidently but not primarily dependent on the increase in the concentration. Furthermore, almost all the results were promising and presented a viability of ≥ 70 %. The primary purpose of the evaluation of cytotoxicity assay on primary macrophages was to find the optimal concentration of the samples for future experiments using human macrophages.

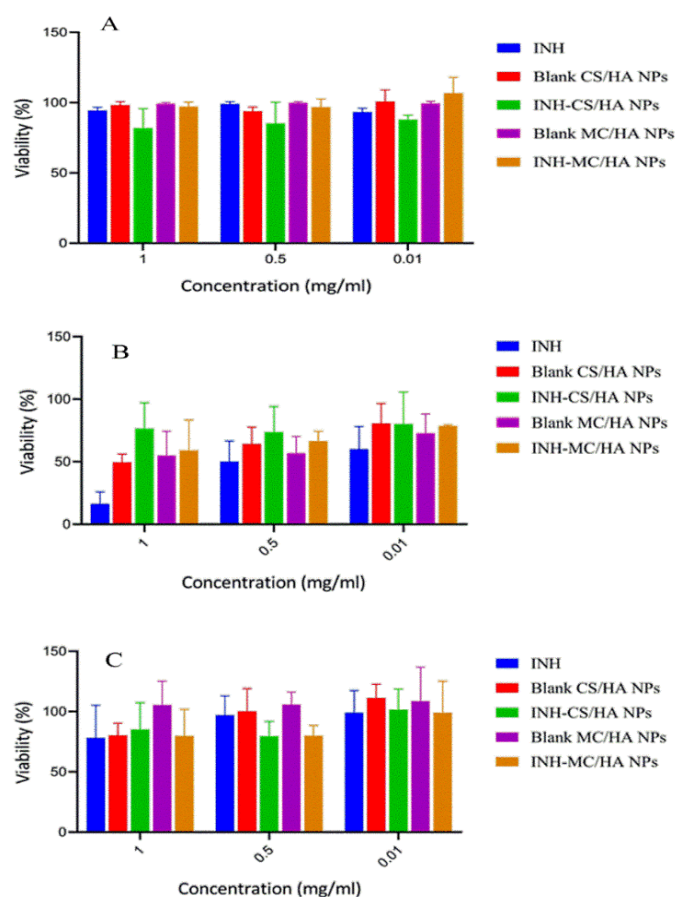


Figure 15: The percentage viability of nanosuspensions on (A) A549 cells, (B) Raw 264.7 macrophages, and (C) primary human macrophages, after an incubation period of 24 h for different concentrations (0.01, 0.5, 1 mg/ml). All the results are expressed as mean \pm S.D, $n=3$

5.10.2 Blood compatibility study

The studies were also performed to validate the compatibility of the formulations with RBCs pivotal to the safety concern. The hemolytic activity was analyzed by the spectrophotometric analysis of plasma-free hemoglobin derivatives, followed by the incubation of nanosuspensions with blood for 4 h and 24 h.

Triton-X serves as a positive control with 100 % cell lysis whereas PBS was used as a negative control with no cell lytic effect (Figure 16). According to ISO/TR 7406, the safe hemolytic ratio for the biomaterials is considered to be less than 5 % [89]. All the nanosuspensions were found to be hemocompatible in the case of this study where none of the samples posed any visible lytic effect on RBCs, irrespective of the incubation period.

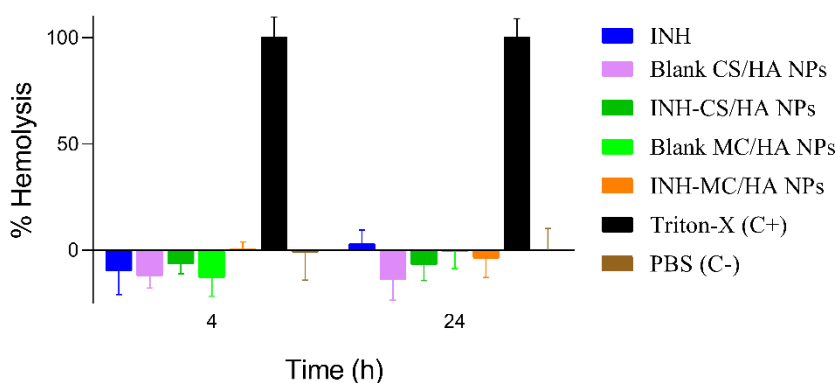


Figure 16: Blood compatibility study performed on fresh human blood, after 4 h and 24 h. The results are expressed as mean \pm SEM, with the results from three different blood donors.

5.10.3 Uptake of nanopowders by macrophages (Qualitative and quantitative)

Figure 17 shows the qualitative visualization of Rh-B labeled NPs inside the A549 cells and Raw 264.7 macrophages by CLSM. The study was performed on A549 cells based on the fact that NPs interact with alveolar epithelial cells before engulfment by macrophages. As it can be seen from the figure, there is a shift in fluorescence intensity after the internalization of NPs inside the cells as compared to the untreated control. The uptake of Rh-B CS/HA NPs was relatively lower in A549 cells and Raw 264.7 macrophages as compared to Rh-B MC/HA NPs. Macrophages are the immune cells responsible for phagocytosis and are more responsive to the uptake of NPs as compared to alveolar epithelial cells. Additionally, there are surface receptors present on the macrophages that play a role in the uptake of NPs.

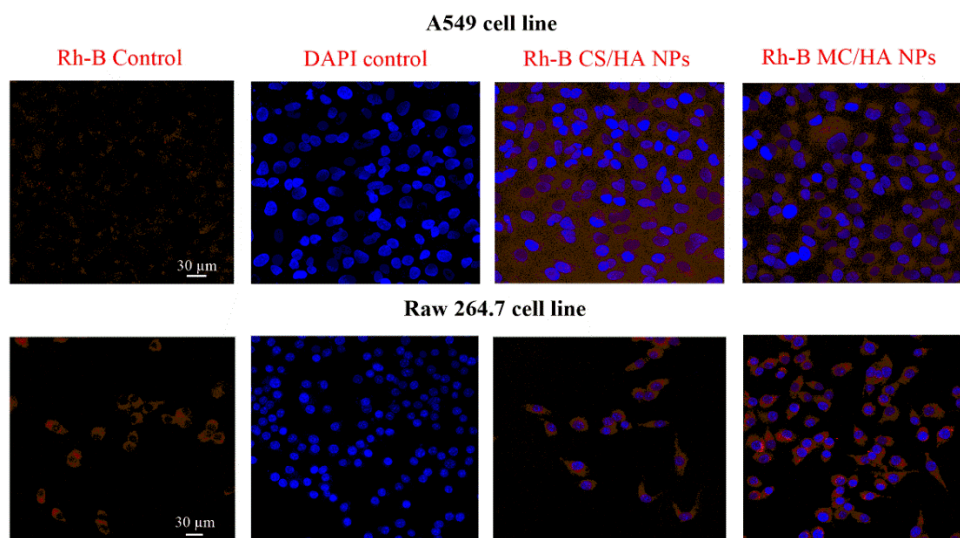


Figure 17: Nanoparticulate uptake study by confocal laser scanning microscopy after an incubation period of 2 h. The red color indicates the fluorescence due to Rhodamine-B dye (Excitation λ_{max} = 546 nm, Emission λ_{max} = 568 nm) and the blue color is indicated the fluorescence due to DAPI-nuclei dye (Excitation λ_{max} = 359 nm, Emission λ_{max} = 457 nm)

This increase in the translocation of the mannose conjugated NPs was also reported in a quantitative study using flow cytometry. It can be observed from figure 18, that after a while of 2 h, there was a relative increase in the uptake of Rh-B MC/HA NPs as compared to Rh-B CS/HA NPs. This established our hypothesis that mannosylation of the polymer can improve the engulfment of NPs in the macrophages.

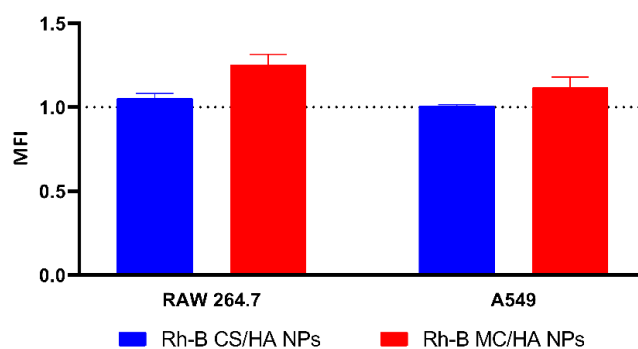


Figure 18: Quantification of uptake of NPs over 24 h by Flow cytometry (Detector FL3, Laser 488 nm, Filter BP 575/25, Software: BD Spectra viewer, Rhodamine B 546/568 (Ex/Em))

5.10.4 Macrophage phenotype analysis

T-lymphocyte costimulatory molecules (CD80 and CD83) are the indicators of pro-inflammatory macrophage-activated phenotype. CD80 influences cytokine expression and

hence is considered a prime co-stimulatory marker [90]. CD80 is also responsible for the expression of interleukin-6 which is involved in the resistance against TB due to its pro-inflammatory nature [91]. Likewise, CD83 levels elevate in the activated macrophage. Moreover, it plays role in the differentiation of T-lymphocytes and tolerance. There is an alleviation of inflammation due to the inhibition of CD83. The expression of CD80 and CD83 was explored by allowing the incubation of macrophages with nanosuspensions for 2 h. The macrophages derived from three different donors were used for the experiment to account for the genetic hematological and immunological differences. The average MFI is represented by a dotted line (Figure 19) which is representing the signals from the macrophages incubated in culture. MFI signals were relatively higher for MC/HA NPs as compared to other samples. Altogether, the results demonstrated the upregulation of the maturation markers and hence the T-cell activation essential to the immune regulation in TB.

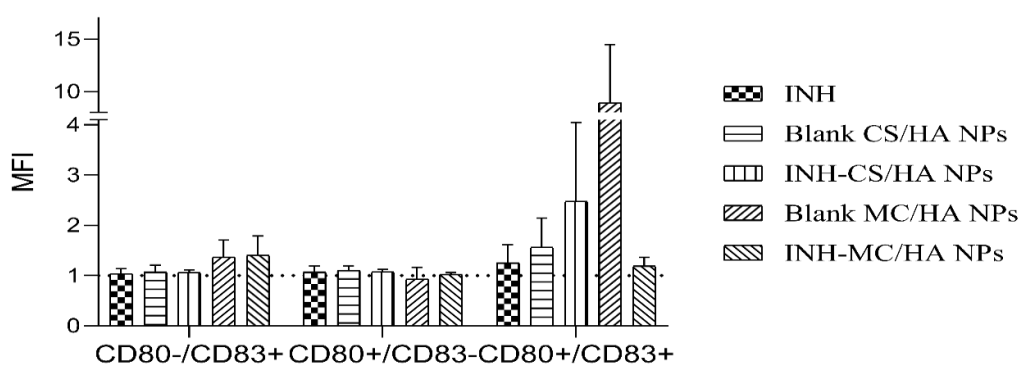


Figure 19: The expression of macrophage maturation markers, CD80 and CD83 as % quantified. The dotted line represents MF=1, which indicates the signal from the incubated macrophages in culture. All the results have been expressed as mean MFI \pm SEM, n=blood from 3 donors

5.10.5 Tolerogenic activity of NPs

Macrophages can affect immune regulation and peripheral tolerance by the IDO expression. Hence, IDO activity was tested by the incubation of nanosuspensions with macrophage cultures (Figure 20).

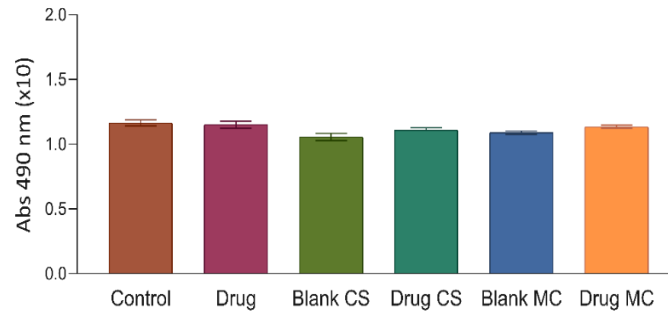


Figure 20: Evaluation of the 2,3-Indoleamine dioxygenase (IDO) after the incubation of nanosuspensions with human macrophage culture

The activation of the tolerogenic phenotype reduces or inhibits the T-cell response and hence the absence of tolerance which is contrary to the pro-inflammatory response. It is worth mentioning that the tolerogenic response suppresses immune regulation in TB. Also, the elevation of tolerogenic activity suppresses effector T-cells and can lead to the immune response tolerance which is not favourable in TB [92]. Interestingly, there was no tolerogenic response recorded for the nanosuspensions similar to that of control (macrophages in culture media).

6. CONCLUSION

Although TB is a curable disease, however, the existing therapies have certain limitations. Already marketed dosage forms fail to deliver the drug to the target site where the causative bacteria reside. Therefore, an adequate drug dose has to be administered to maintain the therapeutic concentration at the target site which however leads to toxicity and drug resistance over time.

Hence, this project aimed to deliver the anti-tubercular to the target site to achieve consistent therapeutic outcomes. Moreover, the concept of nanotechnology was employed to design the delivery system along with a targeted approach.

- After thorough literature review, the polymers employed in this work were selected based on their affinity for the pulmonary epithelial cells and alveolar macrophages having high biodegradability and biocompatibility. MC was synthesized successfully to improve the cellular uptake by exploiting the mannose receptors of macrophages.
- Various critical parameters were studied by QbD and DoE. QbD was implemented to identify the CQAs, CPPs, and CMAs critical to the QTPPs for the preparation of nanosuspensions. The risk assessment indicated the influential parameters which were then studied to acquire the formulations with favorable parameters. Optimization was carried out using time-saving robust DoE that gave an output of the experimental runs to identify the most rational concentrations of polymers. The optimal concentrations of the HA and CS/MC were found to be 5 mg and 2.5 mg respectively. 10 % of the oral dose was encapsulated in the NPs, as established by the literature. And, the sonication speed for the homogenous mixing of the nanosuspension was selected to be 50 pulses per minute.
- The ionic gelation method was employed for the synthesis of nanosuspension which is a very cost-effective and time-saving nanosuspension synthetic approach. Also, Spray-drying and freeze-drying were utilized to obtain the dry nanopowders for inhalation. The PDI for the freeze-dried nanopowders was approximately 0.2 which revealed the highly uniform and narrow size distribution. The results were different in the case of spray-dried nanopowders. Mannitol-based samples were homogenous with the PDI values less than 0.25. Unlikely, the use of Inhalac[®] 400 presented the aggregation in the samples due to the hygroscopic nature of the excipient. The average particle size was 300 nm for the freeze-dried nanopowders.

However, the particle size varied within the range of 299 to 404 nm for the spray-dried samples. The zeta potential values were high for all the nanopowders irrespective of the drying technique.

- All the *in vitro* characterization approaches demonstrated the compatibility among the excipients, polymers, and drug. The aerodynamic parameters of the nanopowders were highly promising in the case of spray-dried MCM with an MMAD of 1.632 and FPF < 5 μm of 80 % among all the samples. However, the drying techniques did not significantly alter the *in vitro* deposition studies and the *in silico* deposition profile. The *in vitro* release profile presented that upon mannosylation, the drug release was slowed down from 63 % to 40 %. Likewise, using MC as a polymer and mannitol as an excipient improved the permeation profile of the nanopowders.
- The nanosystems were found to be biocompatible, hemocompatible, and posed no toxicity to the cells based on the *ex vivo* studies. As the cure to TB involves T-cell stimulation, so the interaction of macrophages with the NPs was also studied to determine the immune response. No immune-suppressive response was exhibited during the studies. Furthermore, no tolerogenic activity was presented by the nanopowders. The T-lymphocyte costimulatory markers CD80 and CD83 were upregulated in the macrophage phenotype study which highlighted the T-cell activation upon the contact of nanosystems to macrophages.

7. NOVELTY AND PRACTICAL ASPECTS

The conventional therapies for TB are failing in the long run due to patient non-compliance as a result of longer duration of therapy, off-site organ toxicity, and economic burden on the patient. Thus, a delivery system with simplicity, safety, scalability, low production costs, and high therapeutic efficacy is the need for an hour.

- The novelty of this work is based on the aspect that all the preliminary regulatory aspects were also explored apart from the pharmaceutical concerns. The thorough literature review gave an insight into the critical aspects of formulation development followed by QbD rational designing.
- The optimization of the formulations through robust DoE is considered a pivotal step toward the application of polymeric-based nanosystems. Developing pulmonary inhalation powders with favorable particle characteristics improved the aerodynamic profile.
- A pulmonary inhalation system developed using nanotechnology combined the promising attributes of nano-dimensional powders and inhalation in a targeted approach toward macrophages in the lungs. The nanosystem prolonged the release of INH in the SLF thereby reducing the dosing frequency and hence the dose-dependent toxicity.
- The method used was cost-effective along with the low cost of natural polymers. The lyophilized powders for injection are already on the market and hence this freeze-dried approach can easily be scaled-up for the pulmonary administration. Moreover, the pulmonary powders available in the pharmaceutical industry employ spray-drying currently. Therefore, both drying approaches can be practical in terms of R&D.
- Several clinical trials using nanotechnology to target macrophages in different diseases are ongoing and awaiting favorable clinical outcomes. This work not only focused on the practical aspects but also the novelty in terms of immune regulation.
- The studies conducted on macrophages presented promising outcomes and therefore provide a foundation for *in vivo* studies in the future.
- Altogether, this pulmonary inhalation approach is innovative in the field of pharmaceutical technology.

8. REFERENCES

1. Fenaroli, F., et al., Nanoparticles as drug delivery system against tuberculosis in zebrafish embryos: direct visualization and treatment. *ACS nano*, 2014. 8(7): p. 7014-7026.
2. Singh, J., et al., Advances in nanotechnology-based carrier systems for targeted delivery of bioactive drug molecules with special emphasis on immunotherapy in drug resistant tuberculosis—a critical review. *Drug delivery*, 2016. 23(5): p. 1676-1698.
3. Mukhtar, M., et al., Aerodynamic properties and in silico deposition of isoniazid loaded chitosan/thiolated chitosan and hyaluronic acid hybrid nanoplex DPIs as a potential TB treatment. *International Journal of Biological Macromolecules*, 2020. 165: p. 3007-3019.
4. Guirado, E., L.S. Schlesinger, and G. Kaplan. Macrophages in tuberculosis: friend or foe. in *Seminars in immunopathology*. 2013. Springer.
5. Mukhtar, M., et al., Drug delivery to macrophages: A review of nano-therapeutics targeted approach for inflammatory disorders and cancer. *Expert Opinion on Drug Delivery*, 2020. 17(9): p. 1239-1257.
6. Russell, D.G., et al., Foamy macrophages and the progression of the human tuberculosis granuloma. *Nature immunology*, 2009. 10(9): p. 943-948.
7. Caws, M., et al., *Tuberculosis in Adults and Children*. 2015: Springer Nature.
8. Winslow, G.M., et al., Early T-cell responses in tuberculosis immunity. *Immunological reviews*, 2008. 225(1): p. 284-299.
9. Costa-Gouveia, J., et al., Combination therapy for tuberculosis treatment: pulmonary administration of ethionamide and booster co-loaded nanoparticles. *Scientific reports*, 2017. 7(1): p. 1-14.
10. Dua, K., et al., Multi-drug resistant *Mycobacterium tuberculosis* & oxidative stress complexity: Emerging need for novel drug delivery approaches. *Biomedicine & Pharmacotherapy*, 2018. 107: p. 1218-1229.
11. Takeda, S.-i., et al., Current surgical intervention for pulmonary tuberculosis. *The Annals of thoracic surgery*, 2005. 79(3): p. 959-963.
12. Geller, D.E., Comparing clinical features of the nebulizer, metered-dose inhaler, and dry powder inhaler. *Respiratory care*, 2005. 50(10): p. 1313-1322.
13. Berger, W., Aerosol devices and asthma therapy. *Current drug delivery*, 2009. 6(1): p. 38-49.

14. Islam, N. and E. Gladki, Dry powder inhalers (DPIs)—a review of device reliability and innovation. *International journal of pharmaceutics*, 2008. 360(1-2): p. 1-11.
15. Patil, T.S., et al., Targeting pulmonary tuberculosis using nanocarrier-based dry powder inhalation: current status and futuristic need. *Journal of drug targeting*, 2019. 27(1): p. 12-27.
16. Vishwa, B., et al., Pulmonary targeting of inhalable moxifloxacin microspheres for effective management of tuberculosis. *Pharmaceutics*, 2021. 13(1): p. 79.
17. Chogale, M.M., S.B. Dhoble, and V.B. Patravale, A triple combination 'nano' dry powder inhaler for tuberculosis: in vitro and in vivo pulmonary characterization. *Drug Delivery and Translational Research*, 2021. 11(4): p. 1520-1531.
18. Miranda, M.S., et al., Exploring inhalable polymeric dry powders for anti-tuberculosis drug delivery. *Materials Science and Engineering: C*, 2018. 93: p. 1090-1103.
19. Kaialy, W., et al., Influence of lactose carrier particle size on the aerosol performance of budesonide from a dry powder inhaler. *Powder technology*, 2012. 227: p. 74-85.
20. Nasiruddin, M., M. Neyaz, and S. Das, Nanotechnology-based approach in tuberculosis treatment. *Tuberculosis research and treatment*, 2017. 2017.
21. Tan, Z.M., et al., Novel approaches for the treatment of pulmonary tuberculosis. *Pharmaceutics*, 2020. 12(12): p. 1196.
22. Dharmadhikari, A.S., et al., Phase I, single-dose, dose-escalating study of inhaled dry powder capreomycin: a new approach to therapy of drug-resistant tuberculosis. *Antimicrobial agents and chemotherapy*, 2013. 57(6): p. 2613-2619.
23. Farhangi, M., et al., Optimization of a dry powder inhaler of ciprofloxacin-loaded polymeric nanomicelles by spray drying process. *Pharmaceutical Development and Technology*, 2019. 24(5): p. 584-592.
24. Benke, E., et al., Stability test of novel combined formulated dry powder inhalation system containing antibiotic: physical characterization and in vitro–in silico lung deposition results. *Drug Development and Industrial Pharmacy*, 2019. 45(8): p. 1369-1378.
25. Sung, J.C., et al., Formulation and pharmacokinetics of self-assembled rifampicin nanoparticle systems for pulmonary delivery. *Pharmaceutical research*, 2009. 26(8): p. 1847-1855.
26. Gaspar, D.P., et al., Microencapsulated solid lipid nanoparticles as a hybrid platform for pulmonary antibiotic delivery. *Molecular Pharmaceutics*, 2017. 14(9): p. 2977-2990.

27. Rawal, T., S. Patel, and S. Butani, Chitosan nanoparticles as a promising approach for pulmonary delivery of bedaquiline. *European Journal of Pharmaceutical Sciences*, 2018. 124: p. 273-287.
28. Rodrigues, B. and P. Shende, Monodispersed metal-based dendrimeric nanoclusters for potentiation of anti-tuberculosis action. *Journal of Molecular Liquids*, 2020. 304: p. 112731.
29. Kulkarni, P., D. Rawtani, and T. Barot, Formulation and optimization of long acting dual niosomes using box-Behnken experimental design method for combinative delivery of ethionamide and D-cycloserine in tuberculosis treatment. *Colloids and Surfaces A: Physicochemical and Engineering Aspects*, 2019. 565: p. 131-142.
30. Grotz, E., et al., Pulmonary delivery of rifampicin-loaded soluplus micelles against *Mycobacterium tuberculosis*. *Journal of Drug Delivery Science and Technology*, 2019. 53: p. 101170.
31. Chan, J.M., et al., Polymeric nanoparticles for drug delivery, in *Cancer Nanotechnology*. 2010, Springer. p. 163-175.
32. Lim, Y.H., et al., Polymeric nanoparticles in development for treatment of pulmonary infectious diseases. *Wiley Interdisciplinary Reviews: Nanomedicine and Nanobiotechnology*, 2016. 8(6): p. 842-871.
33. Moreno, J.A.S., et al., Development of electrosprayed mucoadhesive chitosan microparticles. *Carbohydrate polymers*, 2018. 190: p. 240-247.
34. Huang, Y., et al., Pulmonary inflammation caused by chitosan microparticles. *Journal of Biomedical Materials Research Part A: An Official Journal of The Society for Biomaterials, The Japanese Society for Biomaterials, and The Australian Society for Biomaterials and the Korean Society for Biomaterials*, 2005. 75(2): p. 283-287.
35. Mukhtar, M., et al., Fabrication and optimization of pH-sensitive mannose-anchored nano-vehicle as a promising approach for macrophage uptake. *Applied Nanoscience*, 2020. 10(11): p. 4013-4027.
36. Athamneh, T., et al., Alginate and hybrid alginate-hyaluronic acid aerogel microspheres as potential carrier for pulmonary drug delivery. *The journal of supercritical fluids*, 2019. 150: p. 49-55.
37. Hwang, S., et al., Delivery of ofloxacin to the lung and alveolar macrophages via hyaluronan microspheres for the treatment of tuberculosis. *Journal of controlled Release*, 2008. 129(2): p. 100-106.

38. Nikjoo, D., et al., Hyaluronic Acid Hydrogels for Controlled Pulmonary Drug Delivery—A Particle Engineering Approach. *Pharmaceutics*, 2021. 13(11): p. 1878.
39. Adali, M.B., et al., Spray freeze-drying as a solution to continuous manufacturing of pharmaceutical products in bulk. *Processes*, 2020. 8(6): p. 709.
40. Chang, R.Y.K., et al., Dry powder pharmaceutical biologics for inhalation therapy. *Advanced Drug Delivery Reviews*, 2021. 172: p. 64-79.
41. Emami, F., et al., Drying technologies for the stability and bioavailability of biopharmaceuticals. *Pharmaceutics*, 2018. 10(3): p. 131.
42. Malamatari, M., et al., Spray drying for the preparation of nanoparticle-based drug formulations as dry powders for inhalation. *Processes*, 2020. 8(7): p. 788.
43. Cheow, W.S., S. Li, and K. Hadinoto, Spray drying formulation of hollow spherical aggregates of silica nanoparticles by experimental design. *Chemical Engineering Research and Design*, 2010. 88(5-6): p. 673-685.
44. Li, H., et al., Paeonol loaded cyclodextrin metal-organic framework particles for treatment of acute lung injury via inhalation. *International Journal of Pharmaceutics*, 2020. 587: p. 119649.
45. Littringer, E.M., et al., The morphology and various densities of spray dried mannitol. *Powder technology*, 2013. 246: p. 193-200.
46. Torge, A., et al., The influence of mannitol on morphology and disintegration of spray-dried nano-embedded microparticles. *European Journal of Pharmaceutical Sciences*, 2017. 104: p. 171-179.
47. Adi, H., et al., Co-spray-dried mannitol–ciprofloxacin dry powder inhaler formulation for cystic fibrosis and chronic obstructive pulmonary disease. *European Journal of Pharmaceutical Sciences*, 2010. 40(3): p. 239-247.
48. Velikyan, I., Prospective of ⁶⁸Ga-radiopharmaceutical development. *Theranostics*, 2014. 4(1): p. 47.
49. Guideline, I.H.T., Quality risk management. Q9, Current step, 2005. 4: p. 408.
50. Guideline, I.H.T., Pharmaceutical quality system q10. Current Step, 2008. 4.
51. Yu, L.X., Pharmaceutical quality by design: product and process development, understanding, and control. *Pharmaceutical research*, 2008. 25(4): p. 781-791.
52. Yu, L.X., et al., Understanding pharmaceutical quality by design. *The AAPS journal*, 2014. 16(4): p. 771-783.

53. Draheim, C., et al., A design of experiment study of nanoprecipitation and nano spray drying as processes to prepare PLGA nano-and microparticles with defined sizes and size distributions. *Pharmaceutical research*, 2015. 32(8): p. 2609-2624.
54. Ba-Abbad, M.M., et al., Optimization of nickel oxide nanoparticle synthesis through the sol-gel method using Box-Behnken design. *Materials & Design*, 2015. 86: p. 948-956.
55. Afzal, I., et al., Mannosylated thiolated paromomycin-loaded PLGA nanoparticles for the oral therapy of visceral leishmaniasis. *Nanomedicine*, 2019. 14(4): p. 387-406.
56. Shahnaz, G., et al., Development of mannose-anchored thiolated amphotericin B nanocarriers for treatment of visceral leishmaniasis. *Nanomedicine*, 2017. 12(2): p. 99-115.
57. Sohail, M.F., et al., Folate grafted thiolated chitosan enveloped nanoliposomes with enhanced oral bioavailability and anticancer activity of docetaxel. *Journal of Materials Chemistry B*, 2016. 4(37): p. 6240-6248.
58. Hao, J., et al., Development and optimization of solid lipid nanoparticle formulation for ophthalmic delivery of chloramphenicol using a Box-Behnken design. *International journal of nanomedicine*, 2011. 6: p. 683.
59. Arunkumar, R., K.V.H. Prashanth, and V. Baskaran, Promising interaction between nanoencapsulated lutein with low molecular weight chitosan: Characterization and bioavailability of lutein in vitro and in vivo. *Food Chemistry*, 2013. 141(1): p. 327-337.
60. Jensen, D.M.K., et al., Spray drying of siRNA-containing PLGA nanoparticles intended for inhalation. *Journal of Controlled Release*, 2010. 142(1): p. 138-145.
61. Huh, Y., et al., Preparation and evaluation of spray-dried hyaluronic acid microspheres for intranasal delivery of fexofenadine hydrochloride. *European Journal of Pharmaceutical Sciences*, 2010. 40(1): p. 9-15.
62. Mehanna, M.M., S.M. Mohyeldin, and N.A. Elgindy, Rifampicin-carbohydrate spray-dried nanocomposite: A futuristic multiparticulate platform for pulmonary delivery. *International Journal of Nanomedicine*, 2019. 14: p. 9089.
63. Marques, M.R., R. Loebenberg, and M. Almukainzi, Simulated biological fluids with possible application in dissolution testing. *Dissolution Technol*, 2011. 18(3): p. 15-28.
64. Bartos, C., et al., Formulation of levodopa containing dry powder for nasal delivery applying the quality-by-design approach. *European Journal of Pharmaceutical Sciences*, 2018. 123: p. 475-483.

65. Ambrus, R., et al., Novel dry powder inhaler formulation containing antibiotic using combined technology to improve aerodynamic properties. *European Journal of Pharmaceutical Sciences*, 2018. 123: p. 20-27.
66. Attila, K., *Optikai mérési módszerek fejlesztése és alkalmazása az aeroszolok légúti kiülepedésének vizsgálatára*. 2021.
67. Koblinger, L. and W. Hofmann, Monte Carlo modeling of aerosol deposition in human lungs. Part I: Simulation of particle transport in a stochastic lung structure. *Journal of Aerosol Science*, 1990. 21(5): p. 661-674.
68. Farkas, Á., et al., Experimental and computational study of the effect of breath-actuated mechanism built in the NEXThaler® dry powder inhaler. *International Journal of Pharmaceutics*, 2017. 533(1): p. 225-235.
69. Posch, W., C. Lass-Flörl, and D. Wilflingseder, Generation of human monocyte-derived dendritic cells from whole blood. *JoVE (Journal of Visualized Experiments)*, 2016(118): p. e54968.
70. Scordo, J.M., D.L. Knoell, and J.B. Torrelles, Alveolar epithelial cells in *Mycobacterium tuberculosis* infection: active players or innocent bystanders? *Journal of innate immunity*, 2016. 8(1): p. 3-14.
71. Wu, F., et al., Galactosylated LDL nanoparticles: a novel targeting delivery system to deliver antigen to macrophages and enhance antigen specific T cell responses. *Molecular pharmaceutics*, 2009. 6(5): p. 1506-1517.
72. Clark, A., et al., Cerium oxide and platinum nanoparticles protect cells from oxidant-mediated apoptosis. *Journal of Nanoparticle Research*, 2011. 13(10): p. 5547-5555.
73. Robla, S., et al., A chitosan-based nanosystem as pneumococcal vaccine delivery platform. *Drug Delivery and Translational Research*, 2021. 11(2): p. 581-597.
74. Braun, D., R.S. Longman, and M.L. Albert, A two-step induction of indoleamine 2, 3 dioxygenase (IDO) activity during dendritic-cell maturation. *Blood*, 2005. 106(7): p. 2375-2381.
75. Rager, M.N., et al., ³¹P-NMR and ¹³C-NMR studies of mannose metabolism in *Plesiomonas shigelloides*: Toxic effect of mannose on growth. *European Journal of Biochemistry*, 2000. 267(16): p. 5136-5141.
76. Yao, W., et al., Practical synthesis and characterization of mannose-modified chitosan. *International journal of biological macromolecules*, 2012. 50(3): p. 821-825.

77. Kumirska, J., et al., Application of spectroscopic methods for structural analysis of chitin and chitosan. *Marine drugs*, 2010. 8(5): p. 1567-1636.
78. Shilakari Asthana, G., et al., Mannosylated chitosan nanoparticles for delivery of antisense oligonucleotides for macrophage targeting. *BioMed Research International*, 2014. 2014.
79. Patel, S.S., N.M. Patel, and M.M. Soniwala, Statistical development of a multifunctional directly compressible co-processed excipient using the melt agglomeration technique. *Asian J Pharm Sci*, 2009. 4(6): p. 340-356.
80. Simon, A., et al., Development of a novel dry powder inhalation formulation for the delivery of rivastigmine hydrogen tartrate. *International journal of pharmaceutics*, 2016. 501(1-2): p. 124-138.
81. Islam, P., et al., Chitosan-based nano-embedded microparticles: impact of nanogel composition on physicochemical properties. *Pharmaceutics*, 2016. 9(1): p. 1.
82. Wu, L., et al., Studies on the spray dried lactose as carrier for dry powder inhalation. *asian journal of pharmaceutical sciences*, 2014. 9(6): p. 336-341.
83. Nkanga, C.I., et al., Preparation and characterization of isoniazid-loaded crude soybean lecithin liposomes. *International journal of pharmaceutics*, 2017. 526(1-2): p. 466-473.
84. Thongnopkoon, T. and C. Chittasupho, Curcumin composite particles prepared by spray drying and in vitro anti-cancer activity on lung cancer cell line. *Journal of Drug Delivery Science and Technology*, 2018. 45: p. 397-407.
85. Mehrabi, M., et al., Development and physicochemical, toxicity and immunogenicity assessments of recombinant hepatitis B surface antigen (rHBsAg) entrapped in chitosan and mannosylated chitosan nanoparticles: as a novel vaccine delivery system and adjuvant. *Artificial cells, nanomedicine, and biotechnology*, 2018. 46(sup1): p. 230-240.
86. Craig, R., Intestinal permeability: the cellobiose/mannitol test. *Gut*, 2001. 49(2): p. 312.
87. Kang, M.L., C.S. Cho, and H.S. Yoo, Application of chitosan microspheres for nasal delivery of vaccines. *Biotechnology advances*, 2009. 27(6): p. 857-865.
88. Zhang, Z., et al., Uniform core-shell molecularly imprinted polymers: a correlation study between shell thickness and binding capacity. *RSC advances*, 2014. 4(60): p. 31507-31514.
89. Snima, K., et al., O-Carboxymethyl chitosan nanoparticles for metformin delivery to pancreatic cancer cells. *Carbohydrate polymers*, 2012. 89(3): p. 1003-1007.

90. Maj, T., A. Slawek, and A. Chelmonska-Soyta, CD80 and CD86 costimulatory molecules differentially regulate OT-II CD4⁺ T lymphocyte proliferation and cytokine response in cocultures with antigen-presenting cells derived from pregnant and pseudopregnant mice. *Mediators of Inflammation*, 2014. 2014.
91. Jiménez-Urbe, A.P., et al., CD80 expression correlates with IL-6 production in THP-1-like macrophages costimulated with LPS and dialyzable leukocyte extract (Transferon®). *Journal of immunology research*, 2019. 2019.
92. Mellor, A.L., H. Lemos, and L. Huang, Indoleamine 2, 3-dioxygenase and tolerance: where are we now? *Frontiers in immunology*, 2017. 8: p. 1360.

9. ACKNOWLEDGMENTS

Foremost, I would like to express my gratitude and my utmost appreciation to my supervisor, **Dr. Rita Ambrus** for her kind and continuous assistance throughout my Ph.D. journey. Alongside her continuous financial and scientific supervision, she also had been kind enough to appreciate all my achievements and accept my uniqueness. Without her support, I would not have been able to come so far. I would like to extend my gratitude to **Prof. Dr. Ildikó Csóka** for her assistance and never-ending support as the head of the Institute and in promoting the diverse scientific culture in the Institute of Pharmaceutical Technology and Regulatory Affairs. My sincere appreciation to **Prof. Dr. Piroska Szabó-Révész** for her kind advice and moral support throughout.

A special thanks to **Dr. Noemi Csaba**, Associate professor at the Department of Pharmacology, Pharmacy and Pharmaceutical Technology and Principal Investigator at CIMUS, Universidade de Santiago de Compostela Spain, for her unconditional support and scientific collaboration. I would extend similar gratitude to **Dr. Rubén Varela-Calvino** (Department of Biochemistry & Molecular Biology, School of Pharmacy, Universidade de Santiago de Compostela, Spain) for his unprecedented assistance. I am also thankful to **Dr. Katalin Burián** from the Department of Medical Microbiology and Immunobiology, the University of Szeged for her collaboration. A special thanks to **Dr. Gábor Katona** and **Dr. Csilla Bartos** (Institute of Pharmaceutical Technology and Regulatory Affairs) for their kind help. Special gratitude to **Dr. Árpád Farkas** (Centre for Energy Research, Hungarian Academy of Sciences), **Dr. Zsolt Szakonyi** (Institute of Pharmaceutical Chemistry, University of Szeged), and **Dr. Atilla Nagy** (Wigner Research Centre for Physics, Hungarian Academy of Sciences) for their kind collaboration. Moreover, this research would not have been possible without the loving support of **Piroska Lakatosné** and **Erika Feczóné** for technical support. I would also then like to thank **Dr. Hussain Ali** from the Department of Pharmacy, Quaid-i-Azam University Islamabad, Pakistan. I am also indebted to my **lab colleagues** and the **whole staff** of the institute for sharing smiles during this hard journey that made me feel like a home away from home.

I would also like to acknowledge the financial support of the **Stipendium Hungaricum Program, Ministry of Human Capacities**, Hungary, grant no. 20391-3/2018/FEKUSTRAT. The work was also supported by Gedeon Richter Ltd – GINOP project (2.2.1-15-2016-00007), GINOP-2.3.2-15-2016-00036 (Development and application of multimodal optical nanoscopy

methods in life and materials sciences) and Project No. TKP2021-EGA-32 is financed under the TKP2021-EGA funding scheme.

All the blessings and bounties are alone because of **Allah**. I would like to dedicate this work to the love and unparalleled support of my **father** who is my ideal and taught me to ponder, my **mother** who taught me to be self-sufficient and humble, my **husband** for the amazing long-distance love, never-ending emotional support, care and encouragement, my **nephew** who brought happiness to my life, my **brothers** for always looking up to me, **sisters-in-law** for happy conversations, my **in-laws** for always loving and encouraging me, amazing **friends** for listening to me in the time of sadness and joy and my Hungarian neighbour, **Piroska**, who had been a motherly figure to me and looked after me with immense love.